Palaeogeography, Palaeoclimatology, Palaeoecology 567 (2021) 110279

Contents lists available at ScienceDirect

Palaeogeography, Palaeoclimatology, Palaeoecology

journal homepage: www.elsevier.com/locate/palaeo

Spatio-temporal distribution of Quaternary loess across Central Asia

Yougui Song [a,b,*], Yue Li [a], Liangqing Cheng [a], Xiulan Zong [a], Shugang Kang [a], Amin Ghafarpour [c], Xinzhou Li [a], Huanyu Sun [a], Xiaofen Fu [a], Jibao Dong [a], Yunus Mamadjanov [d], Rustam Orozbaev [e,f], Nosir Shukurov [g], Hamid Gholami [h], Shukhrat Shukurov [g], Mengping Xie [a]

[a] *State Key Laboratory of Loess and Quaternary Geology, Institute of Earth Environment, Chinese Academy of Sciences, Xi'an 710061, China*
[b] *CAS Center for Excellence in Quaternary Science and Global Change, Xi'an 710061, China*
[c] *Department of Soil Science, Gorgan University of Agricultural Sciences and Natural Resources, Gorgan 49138-15739, Iran*
[d] *Research Center for Ecology and Environment of Central Asia (Dushanbe), Dushanbe 734063, Tajikistan*
[e] *Research Center for Ecology and Environment of Central Asia (Bishkek), Bishkek 720040, Kyrgyzstan*
[f] *Institute of Geology, National Academy of Sciences of Kyrgyz Republic, Bishkek, 720040, Kyrgyzstan*
[g] *Institute of Geology and Geophysics, State Committee of the Republic of Uzbekistan on Geology and Mineral Resources, Tashkent 100041, Uzbekistan*
[h] *Agriculture engineering and natural resource, University of Hormozgan, Bandar-Abbas, Hormozgan, Iran*

A R T I C L E I N F O

Keywords:
Geochronology
Palaeomagnetism
Luminescence dating
AMS ^{14}C
Dust activities
Regional differentiation
Tianshan Mountains

A B S T R A C T

Central Asia (CA) is one of the main loess regions in the world and provides important information for the understanding of paleoclimate and paleoenvironmental changes. However, the spatio-temporal variability of the loess distribution is still not fully understood. Combining previous studies with our recent field investigations, we focus on the spatial distribution and ages of loess sediments in CA. Loess sediments are mainly distributed on the windward piedmonts of Central Asian high mountains, e.g. the Tianshan Mountains, Kunlun Mountains, and river terraces, with distinct pedogenic characteristics. The distribution of loess sediments is not only related to atmospheric circulations and regional climate but also closely related to landforms. Based on field observations and the pedogenic environment, we recommend that the loess distribution should be divided into three subregions (Western CA, Northern CA, and Eastern CA), which are approximately coincident with the 60% and 30% winter-half year's precipitation percentage contours, and also correspond to three loess depocenters with thicknesses over 200 m. Paleomagnetic, luminescence dating and AMS ^{14}C geochronology indicated that most of the loess outcrops have developed since the last interglacial-glacial period; although CA loess sediments can span the entire Quaternary period and even extend into the Pliocene. AMS ^{14}C can provide reliable ages for the last 25–30 kyr. Quartz OSL and K-feldspar post-infrared infrared stimulated luminescence (pIRIR) dating techniques, based on well-bleached natural environmental materials, can provide reliable ages younger than 80 ka. The luminescence ages of older samples may be underestimated due to signal saturation problems. Dating of deposits at some elevated locations in CA shows rapid and discontinuous deposition, implying that caution is required in the interpretation of proxies and paleoenvironment. Spatial-temporal distributions of Central Asian loess luminescence ages indicate different clusters in different loess subregions, but generally the periods of strong dust activity occurred during cold glacial periods or stadials. New dating techniques should be developed to enable high-resolution paleoclimate reconstruction.

1. Introduction

Aeolian loess is a wind-blown silt-dominated sediment which covers ~10% of the land surface of the planet. Loess deposits with intercalated paleosols can record the most complete Quaternary terrestrial glacial-interglacial cycles with respect to climate change and atmospheric

* Corresponding author at: State Key Laboratory of Loess and Quaternary Geology, Institute of Earth Environment, Chinese Academy of Sciences, Xi'an 710061, China.

E-mail addresses: ygsong@loess.llqg.ac.cn (Y. Song), liyue@ieecas.cn (Y. Li), chenglq@ieecas.cn (L. Cheng), zongxiulan@ieecas.cn (X. Zong), kshg@ieecas.cn (S. Kang), lixz@ieecas.cn (X. Li), sunhy@ieecas.cn (H. Sun), djb@ieecas.cn (J. Dong).

https://doi.org/10.1016/j.palaeo.2021.110279
Received 19 July 2020; Received in revised form 14 January 2021; Accepted 15 January 2021
Available online 11 February 2021

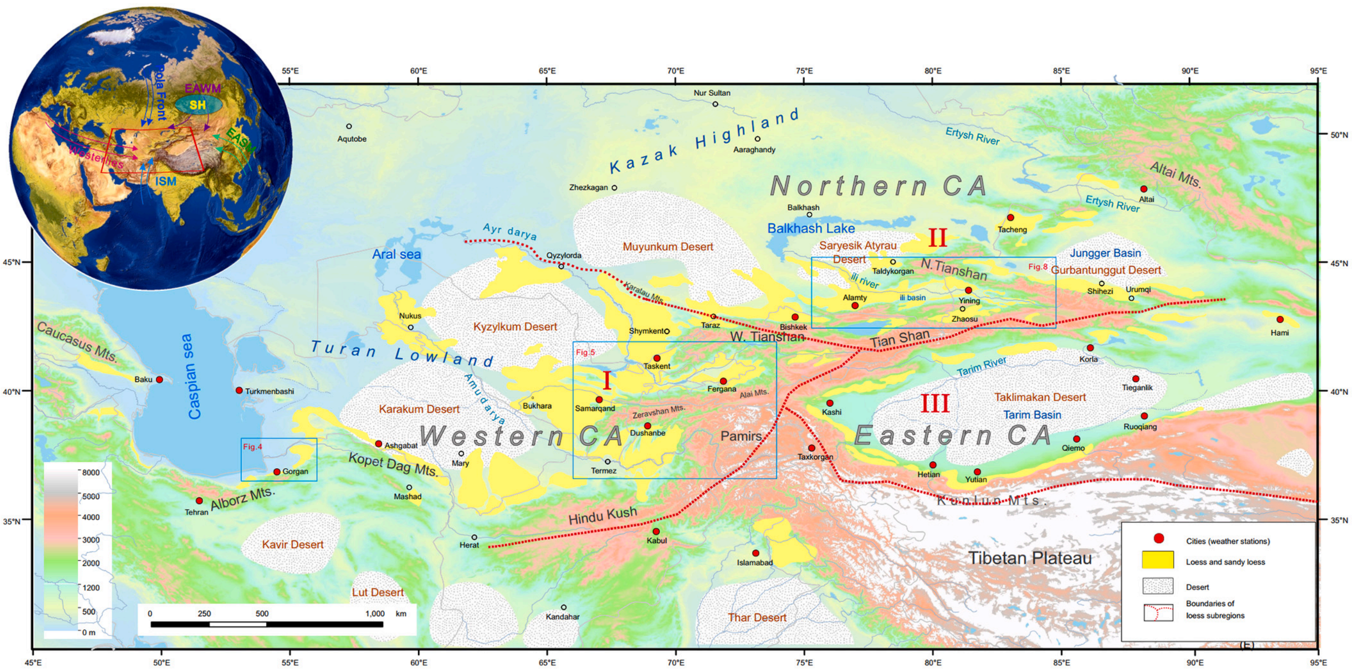

Fig. 1. Schematic map of loess and sandy loess distribution, and locations of meteorological stations in Central Asia.
ISM: Indian Summer Monsoon; EAWM: East Asian Winter Monsoon; EASM: East Asian Summer Monsoon; SH: Siberian High.

circulations over millennial to orbital timescales (e.g.Hao et al., 2012; Heller and Liu, 1986; Heller and Liu, 1982; Muhs, 2013b; Porter and An, 1995; Song et al., 2014b). For example, loess studies of the Chinese Loess Plateau (CLP) have greatly improved our understanding of the spatial-temporal evolutions of the Eastern Asian Monsoon, Asian inland aridification and even past global changes (e.g. Ding et al., 2005; Guo et al., 2002; Lu et al., 2010; Maher, 2016).

Central Asia (CA) is one of the main loess regions in the world, characterized by comparatively patchy piedmont loess deposits of varying thickness (Schaetzl et al., 2018). Loess deposits are one of the most important archives of paleoenvironmental changes, including dust sources, paleoclimatic variability and atmospheric circulation in the Westerlies-dominated CA region. Loess deposits in CA have been studied since the 1990s (e.g. Dodonov, 1991; Dodonov and Baiguzina, 1995; Forster and Heller, 1994; Frechen and Dodonov, 1998; Zhou et al., 1995). However, the spatial-temporal of Central Asian loess deposits and their specific paleoclimatic implications have not yet been as clearly defined when compared to the substantial deposits at the western and eastern extremities of the Eurasian loess belt, despite increased research in recent years (e.g. Fitzsimmons et al., 2018; Jia et al., 2019; Li et al., 2018a; Li et al., 2020d; Li et al., 2018c; Li et al., 2019a; Li et al., 2019b; Li et al., 2019c; Li et al., 2020f; Machalett et al., 2008; Song et al., 2019; Song et al., 2018b; Youn et al., 2014; Zeng et al., 2019).

Loess grain size (GS) and magnetic susceptibility (MS) are amongst the most common physical properties used as proxies for environmental change. Grainsize is regarded as an indicator of near-surface wind intensity (East Asian Winter Monsoon, EAWM) on the CLP (Lu and An, 1998; Vandenberghe et al., 1998; Xiao et al., 1995), although it may also be affected by vegetation coverage, frozen soil development (Li et al., 2018c), transportation direction and source area (Cheng et al., 2020a), as well as wind strength in CA. MS in the CLP is widely used to reconstruct the level of pedogenesis, which is related to climate parameters (precipitation and temperature). It is well known that paleosol layers have a higher MS than that of loess layers; MS has thus been used as a sensitive proxy of the East Asian summer monsoon intensity (An et al., 1991; Evans and Heller, 1994; Heller and Evans, 1995; Heller et al., 1993; Maher, 1998; Song et al., 2012; Zhou et al., 1990), However, in some loess profiles from CA, the MS of the paleosol layer is lower than that of the loess layer (e.g.Chen et al., 2012; Cheng et al., 2020a; Jia et al., 2012; Jia et al., 2013; Kang et al., 2020; Li et al., 2020d; Li et al., 2018c; Li et al., 2020e; Liu et al., 2012; Song et al., 2010; Song et al., 2019; Zeng et al., 2019), without a positive relationship with pedogenesis intensity, perhaps due to the effects of topography (e.g. altitude) and sources. In the mountainous areas, the landform especially altitude produces an important effect on regional precipitation and temperature, and further affects the formation and transformation of magnetic minerals (Song et al., 2010). Magnetic mineral composition of source parent rock also has import contribution on MS enhancements in a weak pedogenesis loess. A recent modern process study (Zan et al., 2020) demonstrates that the spatial variations in the magnetic properties of surface eolian sediments across the northern Tibetan Plateau and the adjacent regions depend largely on regional precipitation and magnetic minerals from the source parent rocks. The temperature has a negligible impact on the variations of the magnetic properties of the surface soil samples(Zeng et al., 2019).

Reliable dating provides a basis for paleoclimatic reconstruction; however, dating results are dependent on the different methods and materials used for dating, which impedes accurate description of the paleoclimatic history and full understanding of the hidden driving mechanisms.

A theoretical model for the genesis of CA loess proposes that the fine-grained particles in the loess were produced by glaciers and rivers in the mountains, transported by rivers into the desert basins, and then subsequently transported back onto the piedmonts (Dodonov and Baiguzina, 1995; Fang et al., 2002a; Fang et al., 2002b; Li et al., 2020f; Machalett et al., 2006; Obruchev, 1945; Smalley et al., 2006). However, the origin of CA loess is mostly inferred from the spatial characteristics of the loess grain size, or present-day air circulation patterns (Li et al., 2012; Li et al., 2015b; Sun, 2002; Ye, 2000). Recent studies have suggested that the loess deposits in the Ili Basin, eastern Central Asia and the Afghan-Tajik Basin are dominated by proximal sources constituted by the alluvial plains and local proluvial fans, whereas rare sediments seldom originated from the large CA deserts (Chen et al., 2021; Li et al., 2018b; Li et al., 2020e; Li et al., 2019b; Zeng et al., 2021). Consequently, the provenance of CA loess is not well known and needs to be ascertained by further investigations. Finally, the complicated topography

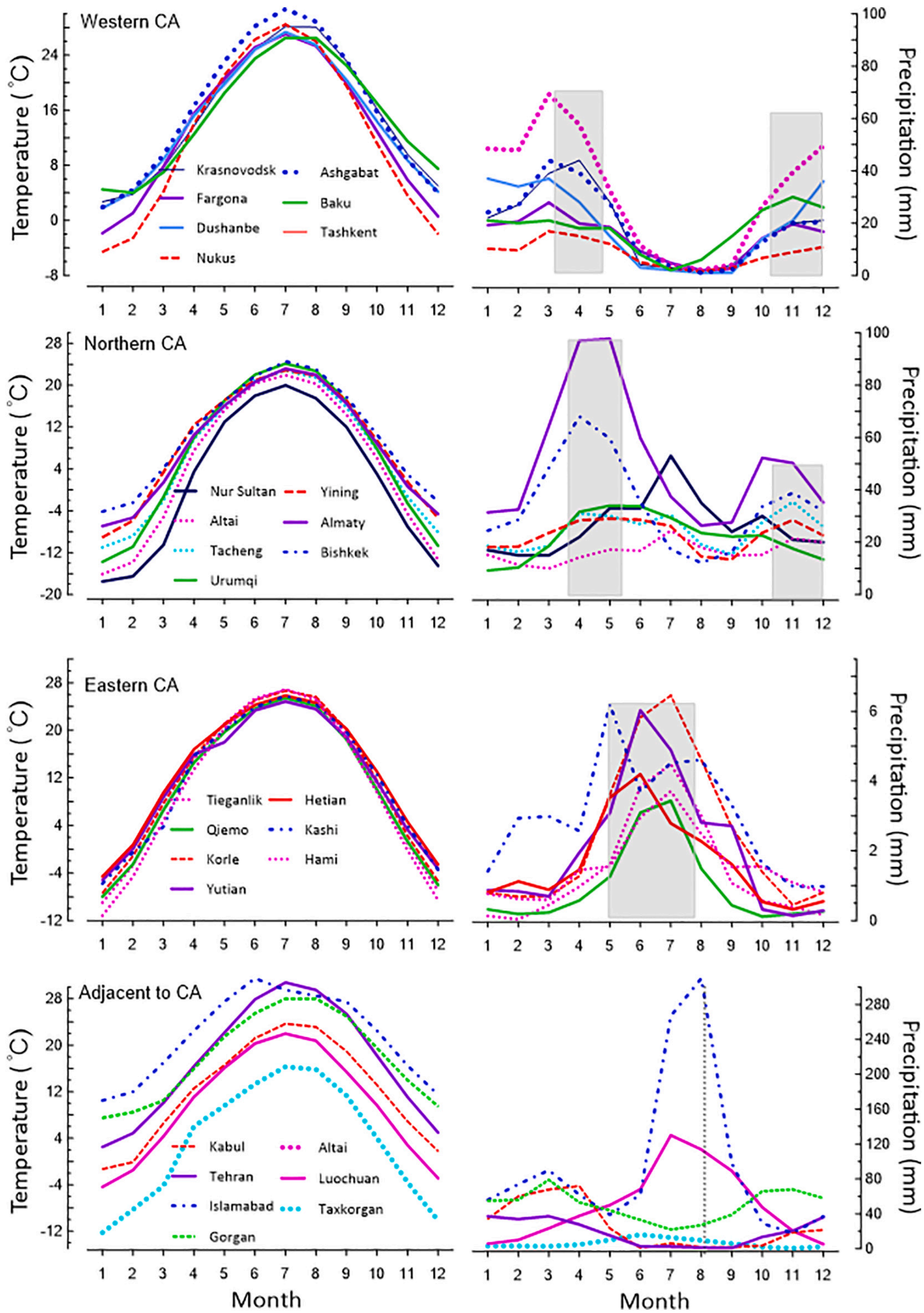

Fig. 2. Mean monthly temperature and precipitation at meteorological stations in Central Asia and the adjacent regions (for locations of meteorological stations, see Fig. 1).

and atmospheric circulation patterns, especially the intensity and location of the Westerlies, strongly affect the climatic features of CA and represent the interactions between the major Northern Hemispheric subsystems of Eurasia over Quaternary timescales (Fitzsimmons et al., 2018; Li et al., 2018c; Machalett et al., 2008; Youn et al., 2014). Thus, climatic trends appear to vary across CA, resulting in markedly different forcing mechanisms (Kang et al., 2020; Li et al., 2020b; Long et al., 2017; Song et al., 2019).

Hence, this study focuses only on the basic problems of the spatio-temporal distribution of CA loess, which is the base of understanding the implication of various proxies and dust sources. The associated climate change and its dynamic mechanisms will be discussed in a future paper.

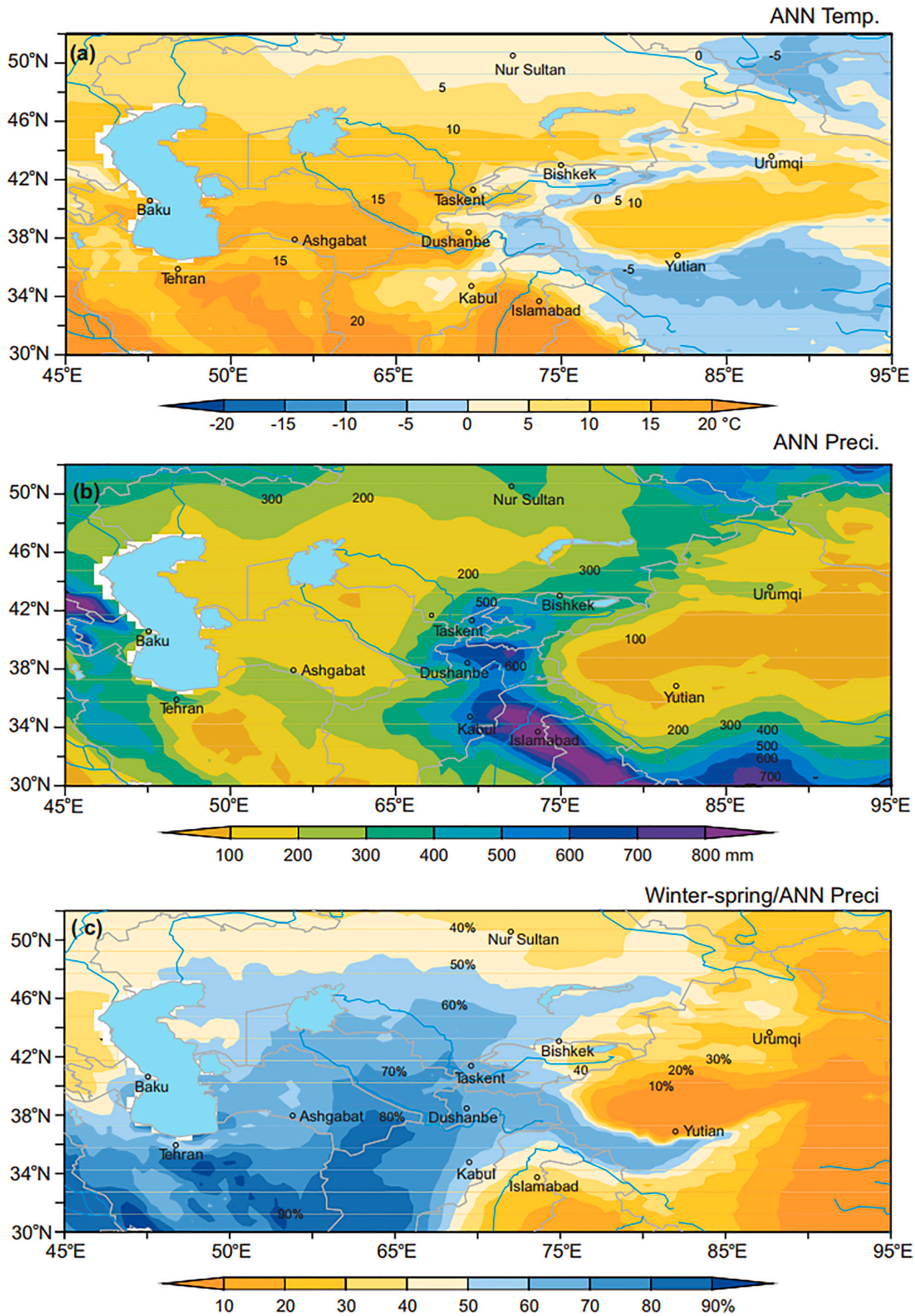

Fig. 3. Annual temperature (a), annual precipitation (b), winter half -year (winter-spring) percentage of annual precipitation (c) in Central Asia.

2. Geographical setting and climate

Central Asia is situated in the hinterland of the Eurasian continent, distant from the sea, extending from the Caspian Sea in the west to China in the east and from the Alborz, Hindu Kush and Pamir Mountains in the south to the Kazak Highlands and Altai Mountains in the north (Fig. 1). This study is focused mainly on the five Central Asian Republics of the former Soviet Union (Turkmenistan, Uzbekistan, Tajikistan, Kyrgyzstan, and Kazakhstan) and the surrounding area, including Xinjiang in China and northern Iran. The topography of Central Asia varies from vast plains and steppes to mountains. The southern and eastern parts of CA are high mountains (e.g. Kopet Dag, Hindu Kush, Tianshan, Altai, Kunlun), interspersed with several basins (i.e. Tajik, Fergana, Ili, Jungger and Tarim). Western CA consists mainly of plains (e.g. Caspian coastal plain and Turan plain) and deserts such as Karakum, Kyzlkum and Muyunkum (Fig. 1).

CA is a landlocked region with a typical continental temperate dry climate, characterized by hot summers and cold winters; seasonality of precipitation varies greatly within the region (Fig. 2). Mid-latitude westerlies (Aizen and Aizen, 1997; Huang et al., 2015; Vandenberghe et al., 2006), the Siberian High (SH) (Feng et al., 2011; Gong and Ho, 2002; Groll et al., 2013; Li et al., 2019a; Sorrel et al., 2007), and the polar front from the north (Machalett et al., 2008), play pivotal roles in the region by affecting moisture advection, while penetration of the East Asian Winter/Summer Monsoon (EASM/EAWM) or Indian Summer Monsoon (ISM) have minor effects (Aizen et al., 1996; Chen et al., 2019; Cheng et al., 2012). Large-scale, distinct, inter-seasonal variations in atmospheric circulations across CA directly influence water vapor transportation (see Fig. S1). Ice core isotope records from the Inilchek Glacier in the central Tianshan Mountains show that 87% of the precipitation originates from the Aral-Caspian (55%) and the eastern Mediterranean and Black Sea (32%) regions; the remaining 13% originates from the North Atlantic Ocean (Aizen et al., 2006). A strengthened Siberian High (SH) pushes the pathways of the mid-latitude westerlies further to the south, resulting in comparably drier conditions in northeastern CA (e.g. Tianshan Mountains), and conversely, wetter conditions in southwestern CA (Pamirs) (Lei et al., 2014; Wolff et al., 2016).

The mountains of the Tianshan, Altai, Hindu Kush and Pamirs have a major impact on the climate and environment of CA (Rugenstein and Chamberlain, 2018; Sha et al., 2018). The mountains act as a significant barrier, not only blocking the entry of warm, wet air currents from the Indian Ocean, but also capturing moisture transported by the Westerlies from the distant Arctic Ocean, Atlantic, and the Mediterranean Sea. The mean annual temperature (MAT) increases from north (5–11 °C) to south (13–16 °C) (Fig. 3a), although topography also has an influence on the MAT, and the mean monthly temperature peaks occur in July (Fig. 2). Over the high rugged mountain ranges, Westerlies-derived air masses bearing recycled moisture are uplifted to produce orographic rainfall (Cai et al., 2017), with low precipitation on leeward slopes and in intermontane basins, resulting in an uneven distribution of precipitation in CA (Fig. 3b). The mean annual precipitation (MAP) in the mountainous areas is higher and increases with rising elevation on windward (west-facing) slopes, reaching 2000 mm in the Fergana Valley (Jilili and Ma, 2015), whereas in deserts, plains and basins is 100–300 mm in western CA, and less than 100 mm in the Taklimakan Desert in eastern CA (Fig. 3b). Seasonal precipitation in CA is also uneven (Fig. 2). Where annual precipitation has spring (major) and winter (minor) peaks (Fig. 2), the proportion of winter half -year (Oct to March) precipitation to annual precipitation is over 60% in western CA (Fig. 3c), but its proportion is less than 30% in eastern CA (Figs. 2, 3c). The precipitation distribution in northern CA is relatively even; the winter half -year precipitation accounts for 30–60% of MAP (Figs. 2,3c), and North Atlantic cyclones are responsible for the most precipitation during the spring-summer period. Therefore, to interpret historical climate data, we have divided the climate pattern of CA into 3 zones. The Western Zone is characterized by hot summer and a mild winter Mediterranean climate with most precipitation occurring during boreal winter (October–April). The Northern Zone is characterized by an arid temperate continental climate with an even distribution of seasonal precipitation. The Eastern Zone is characterized by extreme aridity with hydrothermal synchronization, i.e. high temperature and precipitation occur during summer (June–August) (Figs. 2, 3), indicating monsoonal climate features to some extent.

CA is one of the most important sources of global dust and aerosols. Data obtained from the daily MODIS imagery from 2003 to 2012 showed that dust emissions or dust storms have peaks in spring in the eastern and northern parts of CA, and in summer in the western part (Nobakht et al., 2019). The seasonal disparities of dust emissions are mainly controlled by different atmospheric circulation, which the former is related to Siberian anticyclone (Orlovsky et al., 2005; Roe, 2009). and the latter is related to the Caspian Sea-Hindu Kush Index (CasHKI, defined as the difference in mean sea-level pressure (MSLP) anomalies between Caspian Sea and Hindu Kush)(Kaskaoutis et al., 2016). The Western CA "dust belt", which extends from west to east over the southern deserts, north of the Caspian Sea deserts, Aral Sea region and south of Lake Balkhash, was the major dust emissions source, with a high frequency of dust storms and more prolonged events (Indoitu et al., 2012). Northern CA had less frequent and shorter dust storm events. In eastern CA, the frequency of dust events was smaller by an order of magnitude in the Jungger Basin (10.9 d yr^{-1}) than in the Tarim Basin (111.3 d yr^{-1}). This because that huge amounts of silt materials and a relatively high wind-energy and extreme dry environment in the Taklimakan Desert resulted in more frequent dust events in the Tarim Basin. Floating dust was most frequently observed in the Tarim Basin, which is probably due to the enclosed terrain, while blown dust occurred more frequently in the Jungger Basin.

3. The distribution of Central Asian loess

CA is one of the main dust source regions in the world (Muhs, 2013a), and also one of the main loess distribution regions (Schaetzl et al., 2018). Aeolian dust accumulation (loess) in this area is controlled mainly by topography and atmospheric conditions, especially wind direction and effective moisture. Loess sediments generally accumulate in intermediate locations between the Asian high mountains and the Gobi Desert, particularly on windward slopes, river terraces, alluvial plains and desert margins (Dodonov and Baiguzina, 1995; Machalett et al., 2008; Song et al., 2014a). Sandy loess with several to ten meters is distributed on the edges of the great deserts in CA such as the Taukum, Muyunkum, Kyzylkum, and Saryyesik Atyrau Deserts (Fig. 1), while thick- and silt-dominated loess is distributed closer to the mountains, extending from the foothills of the north Iranian Alborz-Kopet Dag Mountains at their westernmost (Kehl et al., 2005; Vlaminck et al., 2016) extremity, south to the Hindu Kush Mountains-Pamirs Plateau, east to the Northern Tibetan Plateau (Ding et al., 2002b; Dodonov and Baiguzina, 1995), and north along the Altai Mountains margins (Zykin and Zykina, 2015). The piedmont belts of the Tianshan Mountains are the main loess distribution area (Fang et al., 2002b; Fitzsimmons et al., 2018; Song et al., 2014a; Youn et al., 2014); here, the thickness of loess deposits can reach over 200 m in the Ili Basin (Song et al., 2014a), and near 700 m in the pediment of the Kunlun Mountains (Wang et al., 2003; Wu et al., 2020; Zan et al., 2011; Fang et al., 2020).

Based on our field investigations over the last decade and coupled with previous studies (See Supplementary Table 1), we divided CA loess areas into three subregions (Fig. 1), which are approximately consistent with the 60% and 30% winter-half year's precipitation percentage contours (Figs. 1, 3c).

3.1. Western CA loess region (Subregion I)

Subregion I refers to the western CA (or core CA arid region), i.e., from the Caspian Sea to the West Tianshan Mountains - Pamirs Plateau,

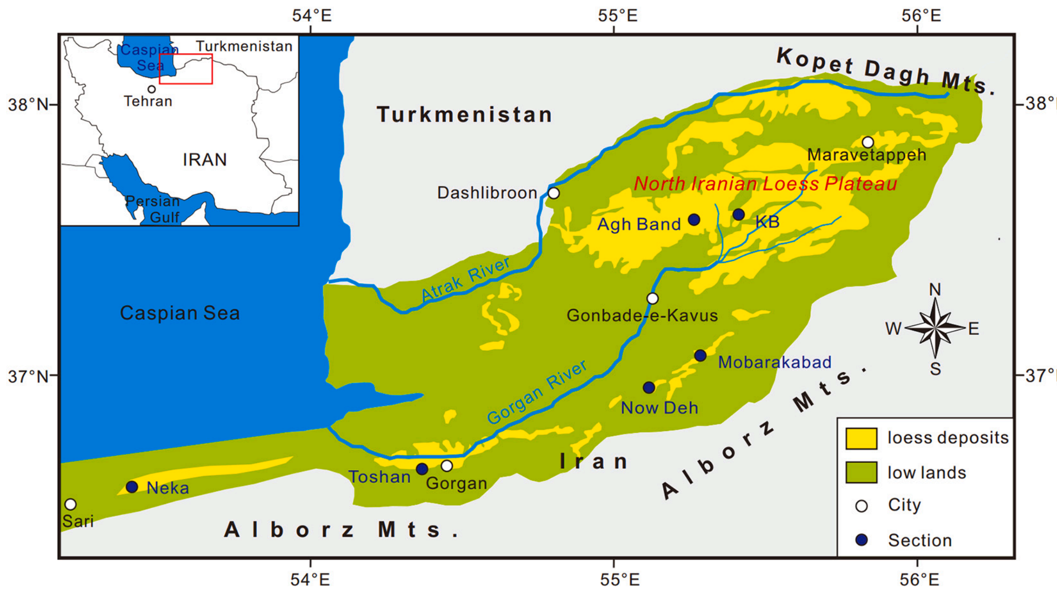

Fig. 4. Loess distribution and reported sections in the North Iranian Loess Plateau (modified from (Asadi et al., 2013) and (Frechen et al., 2009)).

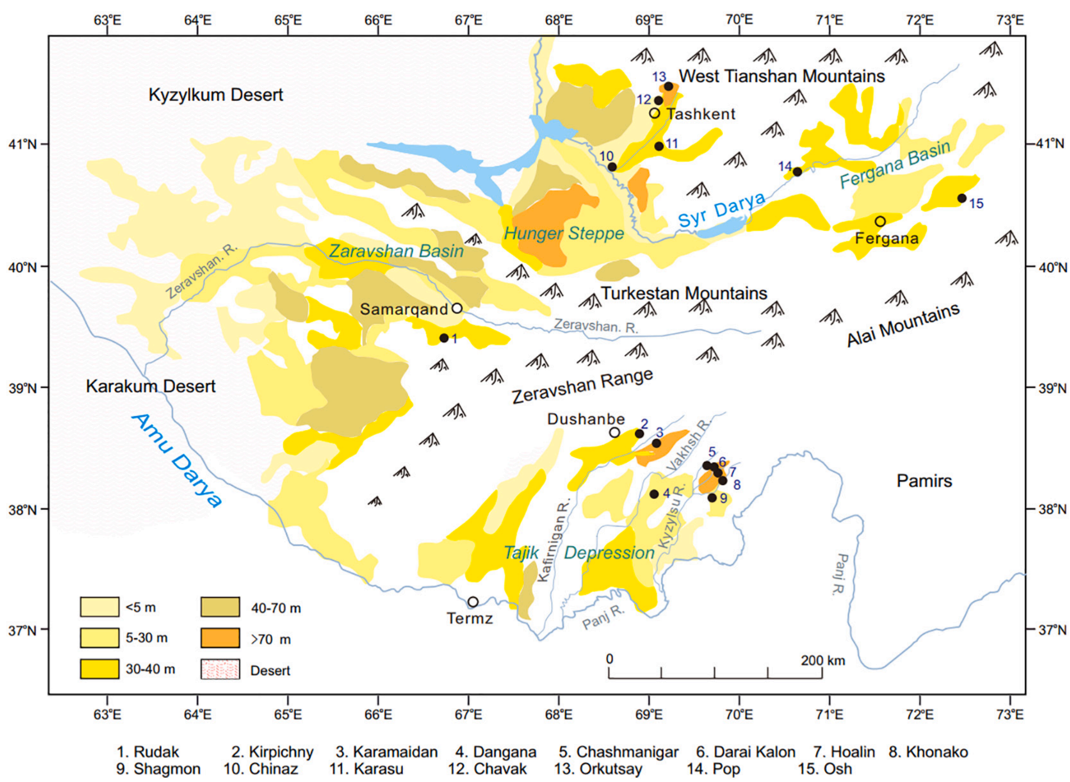

Fig. 5. Sketch map of loess thickness and the studied loess sections in the Tadjik Depression and southeastern Uzbekistan (loess derived from observations and following Smalley et al. (2006)).

including Northern Iran, Turkmenistan, Tajikistan, Uzbekistan and southern Kyrgyzstan. This subregion experiences westerly winds and has a Mediterranean climate, characterized by hot/dry summer and mild/wet winter. The proportion of summer precipitation to annual precipitation is less than 10%. The southern part of the subregion, where annual precipitation is higher (over 600 mm), is also affected by the Indian Summer Monsoon. Loess sediments in the subregion I (Fig. 1) are mainly distributed across the North Iranian Loess Plateau (NILP) (Fig. 4) (Frechen et al., 2009; Kehl, 2010; Lauer et al., 2017a), the Tajik Depression (Penj River valley) (Ding et al., 2002b; Dodonov et al., 2006; Forster and Heller, 1994; Lu et al., 2020), the Zeravashan Basin, the Tashkent-Fergana Basin in eastern Uzbekistan, including Hunger Steppe (Smalley et al., 2006; Zhou et al., 1995), and the western foothills of the Pamirs in southeastern Tajikistan (Ding et al., 2002b; Frechen and Dodonov, 1998) (Fig. 5).

Loess in northern Iran (Figs. 4, 6a) was deposited across a region from the northern foothills of the Alborz Mountains to the Caspian Lowland, and the northeastern slopes of the Kopeh Dagh Mountains. The loess band consists of alternating layers of yellowish loess and moderately well-developed brown paleosols, which were developed during

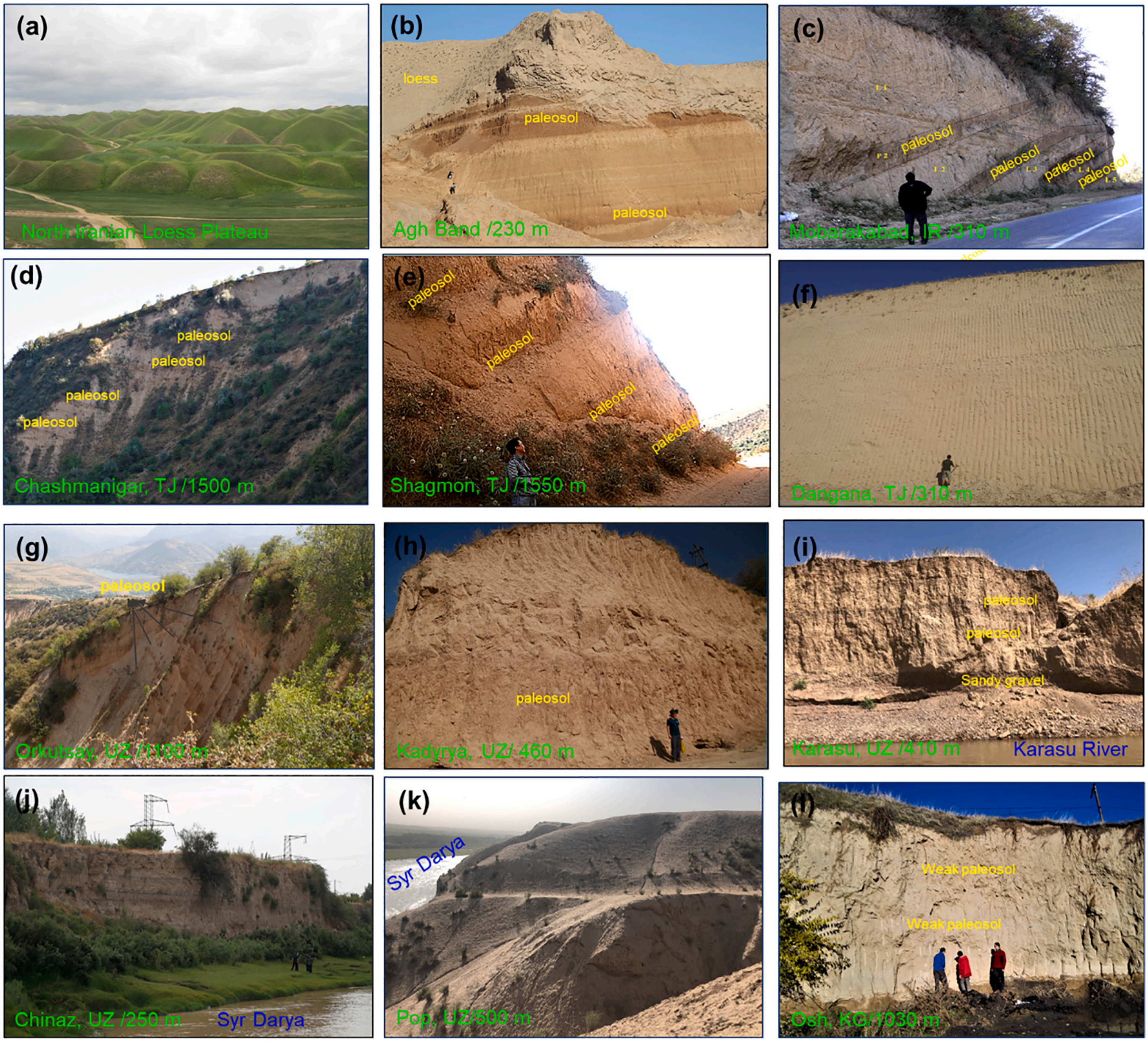

Fig. 6. Loess landscape and sections with elevations in western Central Asia (Subregion I). For the locations of photos, see Figs. 4 & 5; photos in a & c provided by Amin Ghafarpour, photo b by Xin Wang, and other photos by Yougui Song; numbers (m) are elevations.

glacial and interglacial periods, respectively. Because of the arid climate, secondary calcite (up to ~20 cm in diameter carbonate nodules) and gypsum have developed in paleosols (Karimi et al., 2009). In contrast to the paleosol layers, the loess layers have a massive structure and contain small carbonate nodules (<2 cm) with wormholes and Fe-Mn coatings (Wang et al., 2016). The thickness of the loess sediments has a thinning trend from the northeastern to the southwestern NILP along the Gorgan River. The thickness of the loess deposits in the Agh Band (Fig. 6b) exceeds 60 m (Lauer et al., 2017b) and gradually reduces to about 30 m in the Now Deh and Toshan sections towards the southwest (Gorgan) (Frechen et al., 2009; Vlaminck et al., 2018), although the loess thickness in the Neka section, west of Gorgan, exceeds 60 m, with eight intercalated pedocomplexes (PC) (also known as paleosols in the CLP) (Frechen et al., 2009). The total thickness of the Mobarakabad section on the northernmost ridge of the Alborz Mountains (Fig. 4) is about 17 m and contains five PCs (Fig. 6c). Loess deposits in NE Iran cover granitic and meta-sedimentary rocks of the Binaloud Mountain range to the south of Mashhad (Fig. 1), and are thinner (up to 12 m thick) with a patchy distribution (Ghafarpour et al., 2016).

The reaches of the Amu Darya and Syr Darya rivers and mountain piedmonts are the main loess distribution regions in the Tajikistan and Uzbekistan (Fig. 5). Tajikistan possesses the thickest loess layer and the most continuous loess sections in western CA. Thick loess occurs in the Tajik Depression (southern Tajikistan), particularly on the southern piedmonts of the Zeravshan range and southwest of the Altai Mountains, and at the western Pamirs margin (Ding et al., 2002b; Dodonov and Baiguzina, 1995) (Fig. 5). The thickness of loess sediment in the Tajik Depression reaches 200 m (Dodonov et al., 2006). The Darai Kalon section is composed of 18 horizons of PCs with a thickness of 176 m (Dodonov et al., 2006; Frechen and Dodonov, 1998), while the Chashmanigar section is 205 m thick with at least 29 PCs (paleosols) (Ding et al., 2002b; Parviz et al., 2020; Yang et al., 2006) (Fig. 6d). Recent investigation indicated the thickness of the whole Chashmanigar loess section is 220–227 m(Parviz et al., 2020). The thickness rapidly

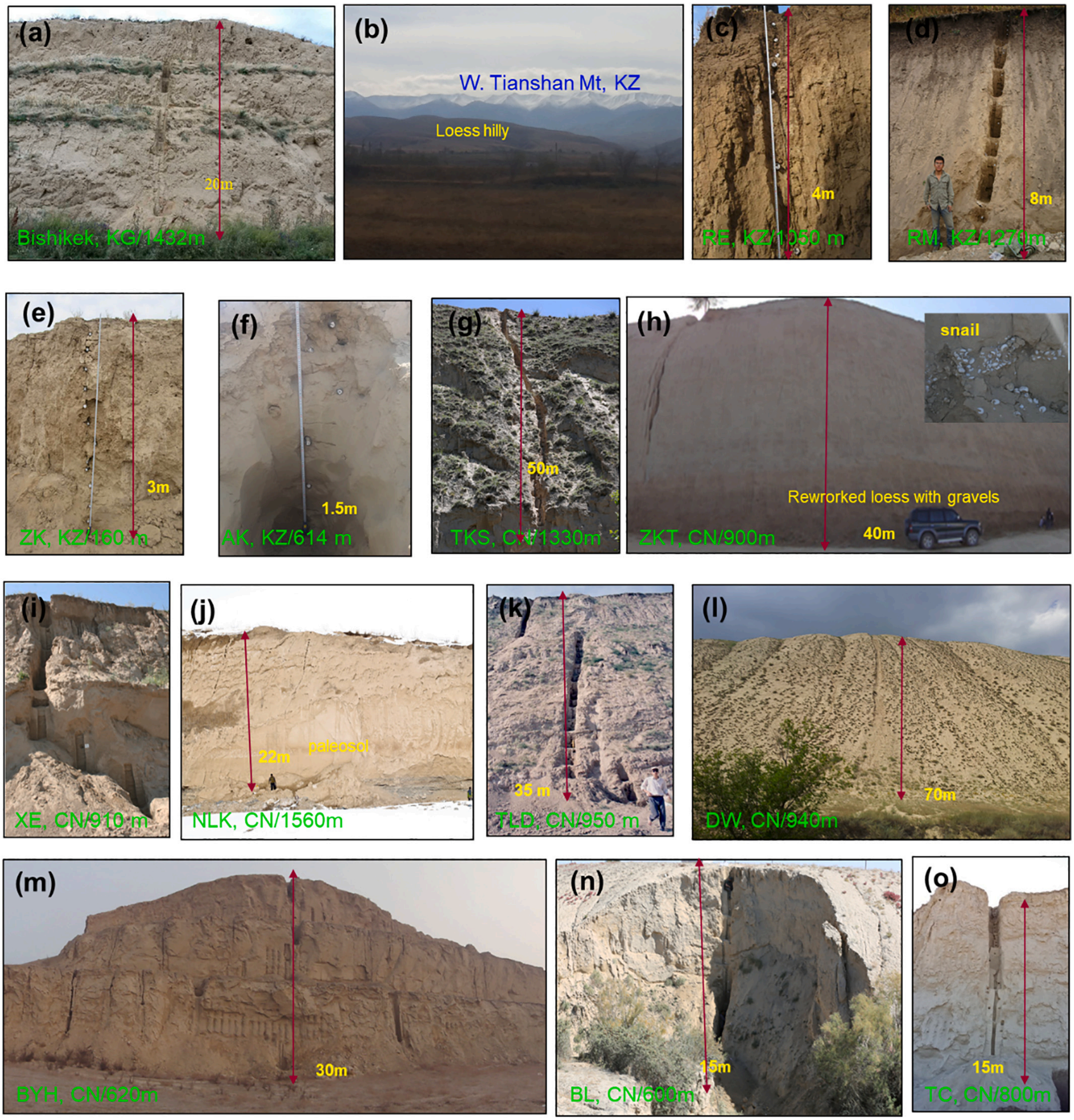

Fig. 7. Loess landscape and sections in Northern Central Asia (photos by Y Song, Y Li).

decreases southward, with no loess along the banks of the Panj River, according to our field investigations in 2015–2017. There is a significant difference in color between loess interbedded with paleosols (Fig. 6e) in this area, and the most loess-paleosol sequences in the Northern Tianshan Mountains are analogous to those of the CLP. Loess layers show a yellowish color, homogeneous silt, with massive structure, while the paleosols are characterized by a brownish or reddish, subangular blocky structure and Fe-Mn clay coatings, which suggest strong pedogenesis. Magnetic susceptibility in the paleosols is higher, in agreement with the loess-paleosol sequences in the CLP (Ding et al., 2002a; Ding et al., 2002b; Yang et al., 2006). Carbonate nodule horizons are also observed below the paleosols; however, no obvious paleosols are observed in the sections in lower elevation areas (Fig. 6f).

In the Tashkent-Fergana Basin, loess mainly covers the piedmont slopes of the west Tianshan Mountains (Fig. 6g) and terraces of the Syr Darya river and its tributaries (Fig. 5), e.g., Chichiq River (Fig. 6h), Karasu River (Fig. 6i). The loess thickness ranges from several meters to 30–50 m (Fig. 6i, k), and up to 100 m at Orkutsay (Fig. 6g), becoming thinner eastwards in the Fergana Basin. The thickness reaches several meters near Osh, with weak pedogenesis (Fig. 6l). Previous studies (Mavlyanov et al., 1987; Smalley et al., 2006) have reported that the Hunger Steppe between the Turkestan Mountains and Syr Darya River has a depocenter with >70 m thickness of loess, or loess-like deposits (Fig. 5). These may be alluvial-proluvial sediments originating from the

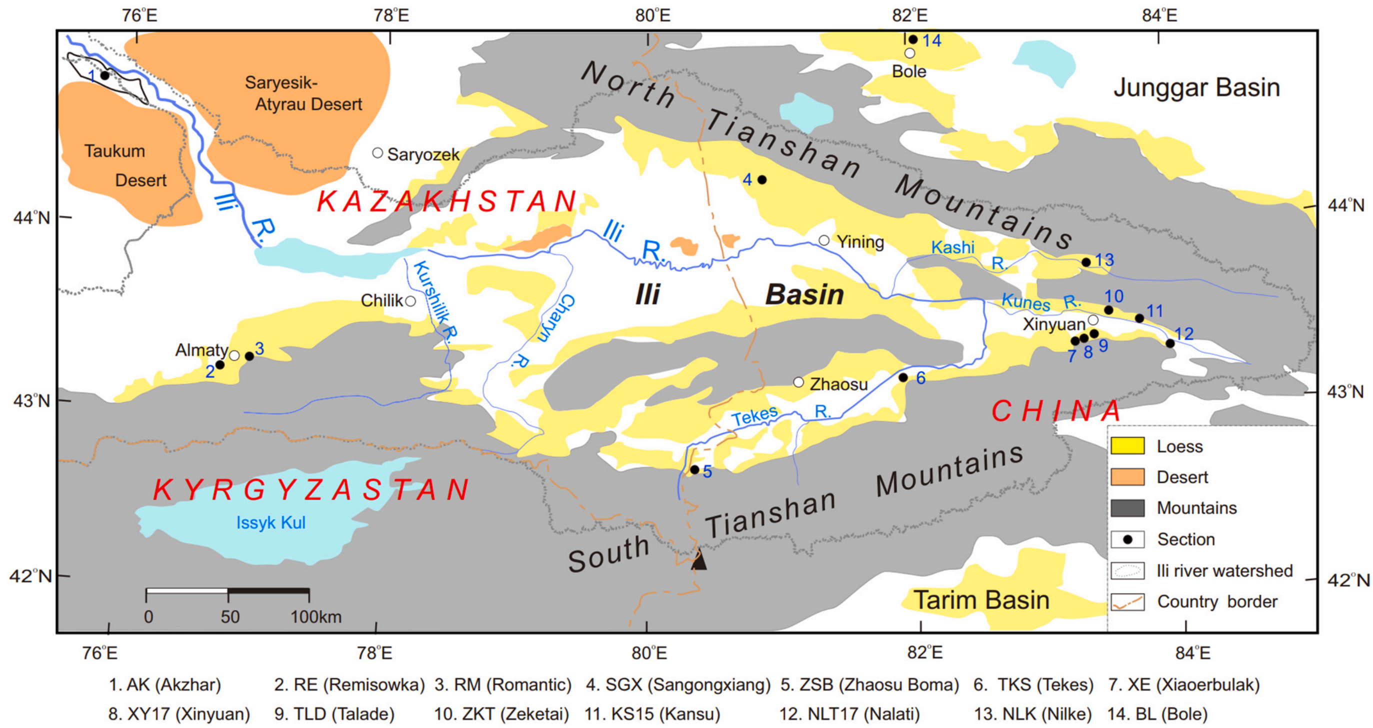

Fig. 8. Loess distribution and loess sections in the Ili River watershed (loess distribution modified from Song et al. (2014a); for photos of sections, see Fig. 7).

Syr Darya river. The Zerafshan Basin is also covered by loess with thicknesses of several meters to ten meters, with no obvious paleosol horizons. There are up to 20 m alluvial-delta loess-like deposits with sand and clay intercalations with thicknesses of near Nukus in the Turan Lowland and along the edges of the Karakum and Kyzylkum Deserts (Fig. 1).

3.2. Northern loess region (Subregion II)

Subregion II is located north part of the Tianshan Mountains, including southeastern Kazakhstan, the Ili Basin, Tacheng Basin and the Altai region of Xinjiang Province, China (Fig. 1). The subregion is influenced by the Siberian High and the Arctic Polar Front. The mid-latitude Westerlies shift northwards in summer, and summer precipitation accounts for 20–50% of total annual precipitation. Loess on the northern slopes of the Tianshan Mountains has been deposited on various geomorphic surfaces, mostly between 700 and 2400 m a.s.l., but there is little to no loess above the forest line. Pedogenesis is weaker in this subregion, hindering the identification of the paleosol layers at lower altitudes (below 1400 m a.s.l.) in the piedmonts. However, the paleosols on mountains at high elevation with higher annual precipitation have a conspicuous brown or reddish color with higher magnetic susceptibility (Song et al., 2010; Song et al., 2014a). Holocene paleosol horizons with strong pedogenesis can be observed in high mountains (Duan et al., 2020).

Field observations in recent years have shown that Kyrgyzstan loess is mainly distributed in the Chu Valley and along the edges of the high-elevation, glaciated Tianshan Mountain ranges in northern Kyrgyzstan. The thickness of the outcropped loess ranges from several meters to 20 m (Fig. 7a). The loess in Kazakhstan is mainly distributed on the windward piedmont of the Tianshan and Karatau Mountains (Fig. 7b–d), river terraces (Fig. 7e), alluvial fans, and along the margins of the Muyunkum, Taukum (Fig. 7f), and Saryesik-Alyrasu Deserts in southeastern Kazakhstan (Fig. 1). The silty loess is distributed at altitudes between 750 and 2400 m a.s.l.; particularly in the foothills of the Tianshan Mountains, where the loess reaches a thickness of up to 100 m, forming a smooth, undulating landscape (Dodonov, 1991; Fitzsimmons et al., 2020; Machalett et al., 2006). The most continuous loess deposits lie west of Almaty and the Ili Gate (Schaetzl et al., 2018). In the middle reaches of the Ili Valley, loess cover is more limited and discontinuous, and more frequent on the southern than the northern slope (Fitzsimmons et al., 2020). The thickest loess section, reported by Machalett et al. (2006), is the Remisowka loess section located in the vicinity of the northwestern Tianshan Mountains near Almaty, which is 80 m thick. The upper 48 m of this section consists of 9 loess layers with numerous mollusc shells and 8 pedocomplexes. Fe-Mn coating, carbonate mycelium, carbonate and gypsum concretions were also observed in this section. The sandy-loess or loess-like sediments found in the river and deserts are thinner, having a thickness of several meters, and are coarser in grain size with polygenetic sources.

In the Ili Basin, loess covers the river terraces of the upper and middle reaches of the Ili River and its tributaries (Kunes, Tekes, Kashi Rivers) (Fig. 8) and extends across the southern and northern slopes of the Tianshan Mountains and the edge of the deserts, ending at the tree line (Song et al., 2014a). The loess sediments are characterized as yellowish or grayish yellow, homogeneous, loose, porous, and fine-medium silt. Terrestrial snails and carbonate concretions are widespread in loess deposits in the southeastern Ili Basin, e.g. the TKS (Fig. 7g), ZTK (Fig. 7h), XE (Fig. 7i), NLK (Fig. 7j), TLD (Fig. 7k) sections. Paleosols are mostly characterized as light brown or taupe, dense, weakly developed with white mycelium patches. Pedogenic accumulation of secondary carbonate or gypsum concretions have developed in paleosol. Some loess-paleosol strata, especially at the bottom, contain gravel and sand, showing the characteristics of multiple genetic processes. The distinction between loess and paleosol in the western Ili Basin, with an arid climate and low altitude, is generally inconspicuous. Pale-brownish weakly-developed paleosols are observed in mountainous regions with high precipitations, e.g. the NLK section (Fig. 7j). The steppe top soil is homogenous and saline with many fine fossil root channels. The thickness of loess deposits ranges from several meters to approximately 200 m. There are two primary depocenters, around Sangongxiang (SGX) and Xinyuan in the central-western Ili Basin (Fig. 8), where 96 m and 202 m drilling cores, respectively, were retrieved, (Song et al., 2014a). The thickness of outcrop loess profiles exceeds 40 m near Zeketai (ZKT) town

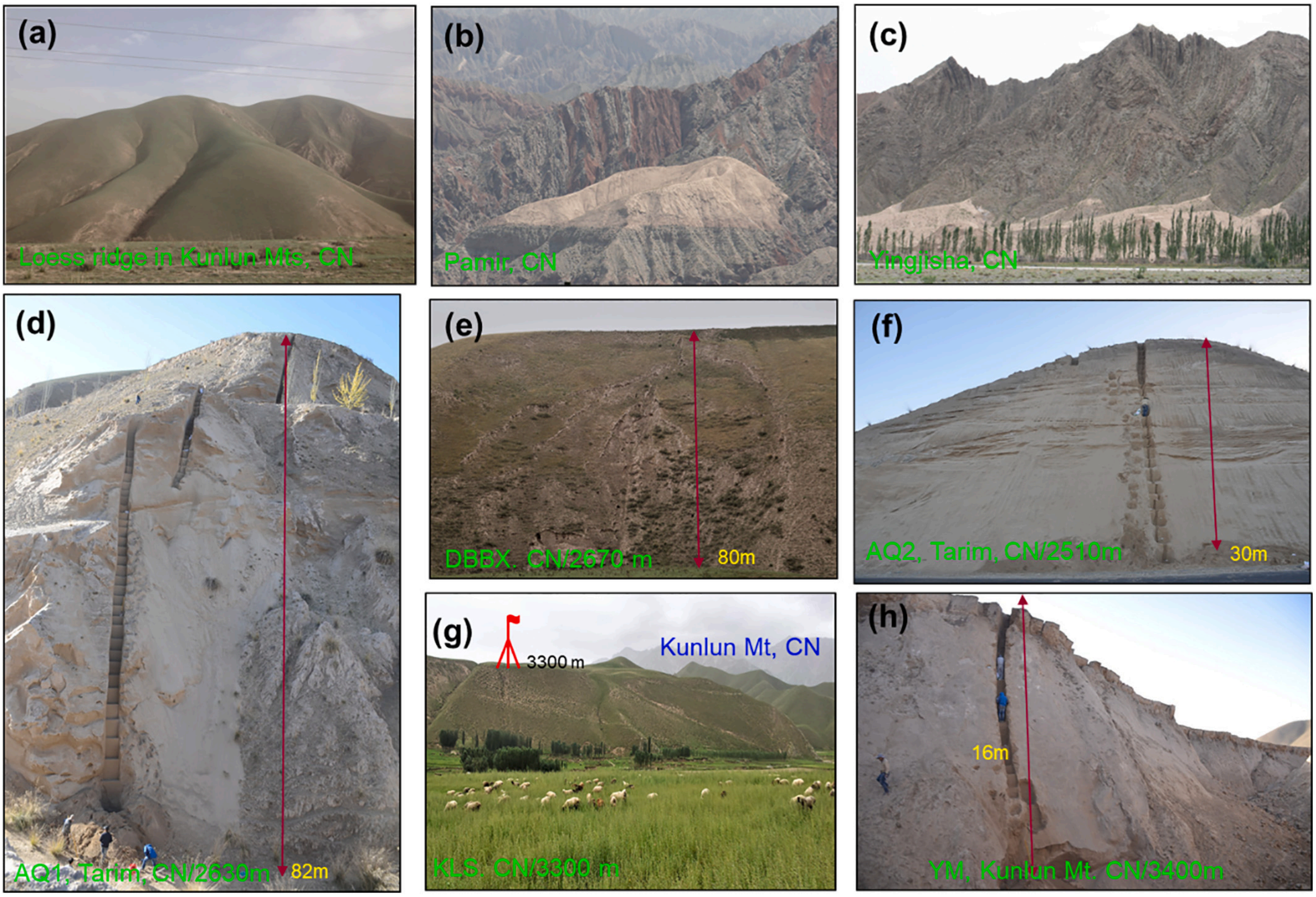

Fig. 9. Loess sections in eastern Central Asia (photos by Yougui Song).

(Fig. 7h) and Talede (TLD) town (Fig. 7k), Xinyuan County, where the altitude is generally 900–1500 m. On the second terrace of the Kashi River, the thickness of loess is more than 20 m at elevations of 1250–1700 m (Fig. 7j) (Li et al., 2018c). The thickness of loess is less than 20 m in Gongliu County at altitudes of 600–1600 m. Loess covers the terraces of the Tekes River at elevations between 1300 and 2100 m, and its thickness varies from a few meters to tens of meters: e.g., the TKS section is about 50 m thick (Fig. 7g) in the Zhaosu sub-basin.

Aeolian loess is widely distributed in the various geomorphic surfaces (e.g. terraces and foothills) between 700 and 2400 m a.s.l. (Fang et al., 2002b), and forms a loess belt along the southern margin of the Junggar Basin and below the fir-spruce forest on the northern slopes of the Tianshan Mountains, mainly from Urumqi to Bole (Fig. 1). The loess thickness ranges from 5 m to 50 m and can even reach up to ~90 m thickness in the Shihezi region. To date, the thickest loess outcrop section observed in this region is about 71 m near Dongwan town (DW) (Fig. 7i), with nine layers of weakly developed paleosol complexes(Fang et al., 2002b; Li et al., 2020c). Loess in this section is characterized by dark yellow, loose, massive structure with many biological relics and intercalated gray yellow loessic sands, and paleosol is brownish gray or brown color, massive structure with many biological channels, carbonate spots and small nodules. There are no gypsum or Fe-Mn coatings. The thickness of loess near Urumqi exceeds 30 m (Fig. 7m). In the Bole region, the thickness of loess increases from west (2–3 m) to east (50–60 m), near Bole city (Fig. 7n). In the Tacheng Basin, the thickness of loess varies from a few meters to 30 m (Fig. 7o) (Cheng et al., 2020a; Li et al., 2015b; Li et al., 2019c). Loess in the north makes a belt zone along the southern foothills of the Tarbagatai Mountains; the loess in the south is mainly distributed in the northern piedmonts of the Barluk Mountains, with an elevation of 800–1200 m. Loess and loess-like sediments are also distributed between the Irtysh River and the southern slopes of the Altai Mountains (Fig. 1).

3.3. Eastern loess region (Subregion III)

The Eastern Loess Region (Subregion III) covers the Tarim Basin (including the Taklamakan Desert and Lop Nor) and its surrounding area. The climate of this subregion is extremely arid, with hydrothermal synchronicity in summer. Loess or loess-like sediments are spread from Kashi in the west to Ruoqiang in the east and constitute a loess belt to the northern slopes of the Kunlun Mountains between 1500 and 4500 m a.s.l. (Fig. 1). The loess landforms are characterized by loess ridges, which have been eroded by rivers (Fig. 9a). From alluvial/proluvial fan, to piedmonts (Fig. 9a) to high mountains (Fig. 9b,c), the thickness of loess follows a thin-thick-thin lenticular pattern and the grain size of sediments gradually decreases. Convergent winds in the Hetian and Yutian regions cause deposition of the thickest loess sediments. The thickness of outcropped loess near Aqiang town in the front of the Kunlun Mountains ranges between 30 and 80 m (Fig. 9d–f). Nine paleosol complexes were reported from an 81 m thick loess section (DBBX) (Fig. 9e) (Fang et al., 2002a) on the slopes of the Kunlun Mountains. However, drilling cores from the loess watershed of the Keriya River near Pulu (about 3300 m a.s.l.) indicated that the thickness can reach 671 m (Fang et al., 2020) (Fig. 9g), although the thickness reduces with increasing elevation; for example, the loess thickness is only 16 m at 3600 m a.s.l. near Yamei village (Fig. 9h). Ten paleosols layers were observed in a 207 m pilot core (Zan et al., 2013; Zan et al., 2010). Thin loess and loess-like sediments occur sporadically between the Tarim River and the southern

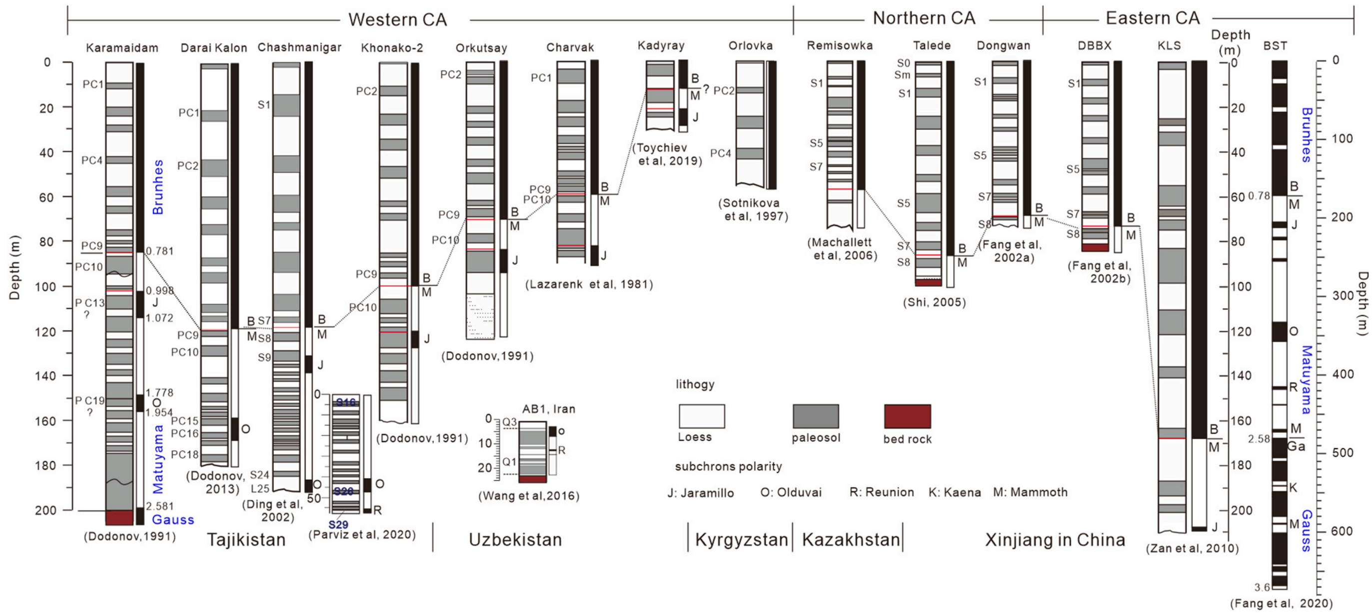

Fig. 10. Magnetostratigraphic correlations of Central Asian loess sections and cores.

slopes of the Tianshan Mountains (Fig. 1).

Loess in this subregion is characterized by gray to light grayish -yellow in color, homogeneous, coarse silt and fine sand. Pedogenesis is generally very weak; it is difficult to recognize the paleosol layers in the field, but it can be distinguished with careful examination and by proxies. It has been generally acknowledged that dust materials originate from proximal deserts and fluvial-alluvial fans. It is believed that loess is a synchronous near-source product from the Taklimakan Desert (Fang et al., 2002a). However, new data sets on the grain size and geochemical studies suggest that the Kunlun Mountains are the main source of the sand fraction, and both the Kunlun and Tianshan Mountains are the main sources of the dust fraction (Jiang and Yang, 2019; Li and Song, 2020).

4. Loess dating in Central Asia

Independent and reliable timescales are prerequisites for Quaternary climate and environmental reconstructions. Since the 1980s, many researchers from Russia, China, UK and Germany have carried out studies on geochronological studies of CA loess, including paleomagnetism and thermoluminescence (TL) dating (e.g. Ding et al., 2002b; Dodonov, 1991; Dodonov and Baiguzina, 1995; Dodonov et al., 1999; Forster and Heller, 1994; Shackleton et al., 1995; Smalley et al., 2006; Zhou et al., 1995). Recently, Infrared Stimulated Luminescence (IRSL), Optically Stimulated Luminescence (OSL) and Accelerator Mass Spectrometry (AMS) ^{14}C have been widely used to date the Middle-Late Quaternary sediments in CA, although controversy remains regarding the reliability of results because of their age inconsistencies and discrepancies (e.g. Kang et al., 2015b; Li et al., 2015a; Li et al., 2016b; Qin and Zhou, 2018; Song et al., 2015; Song et al., 2012; Song et al., 2018b; Wang et al., 2018; Youn et al., 2014). Here, we collected dating results over 30 loess sections or drilling cores from CA (See Supplementary Table 1) and analyses their temporal-spatial distribution characteristics.

4.1. Paleomagnetic dating and formation age of Central Asian loess

The paleomagnetic method was the earliest dating technique used to establish long-term (> 0.8 Ma) geochronological series of loess sediments. The previous magnetostratigraphic correlation has shown that the oldest loess in Tajikistan began to accumulate since Gauss polarity period (2.5 Ma, now 2.6 Ma) at the Karamaidam section, and the Brunhes/Matuyama (B/M) boundary was recognized between PC9 and PC10, the Jaramillo subchron between PC15 and PC16, and the Olduvai subchron was found at the level of PC33 and PC34 (Dodonov and Penkov, 1977). However, the stratigraphic position of the lower outcrop of this section was questioned by the subsequent field investigation(Forster and Heller, 1994), because of the outcrop's stratigraphic position paleomagnetic results of this part seemed to be rather uncertain and could lead to misinterpretation. Further lithological and magnetostratigraphic results (Forster and Heller, 1994; Frechen and Dodonov, 1998) revealed the upper 100 m loess sequence is composed of 13 intervening PC, and confirmed that he B/M boundary is in L10 between PC9 and PC10, but the Jaramillo subchron was located L14 between PC13 and PC14, and the Olduvai subchron was located at L20 of PC19 and PC20 (Frechen and Dodonov, 1998). The subsequent field investigations found that the stratigraphic position of the sections, which Dodonov and Penkov (1977) had interpreted as originating from the late Gauss to the late Matuyama, seemed to be rather uncertain and could lead to misinterpretation (Forster and Heller, 1994). The stratigraphies of these sections in Tajikistan do not compare well with each other (Fig. 10), for example, locations of B/M boundaries are different in the Karamaidam, Darai Kalon and Khonako-2 sections below or above PC9 (Dodonov, 2013; Dodonov, 1991) (Fig. 10). These sections are very close, but have different loess-paleosol couplets. The Chashmanigar section (Fig. 6d) is 195 m thick with 29 loess-paleosol couplets, corresponding to S0-S24 of the Chinese loess. The bottom paleomagnetic age is estimated at 1.77 Ma (Ding et al., 2002b). Recent paleomagnetic analysis (Parviz et al., 2020) extended the basal age of the Chashmanigar section to 2.13 Ma about the Reunion subchron, and paleosol at the bottom of this section was traced back to S29 based on correlation of grain size, magnetic susceptibility with deep-sea oxygen isotope records.

The Darai Kalon section (176 m) with 18 PCs reaches up to 1.1 Ma (Dodonov, 2013) in paleomagnetic age, but the 205 m thick Karamaidam section covers the whole Quaternary. Paleomagnetic and fossil assemblages suggest there are Upper and Middle Pleistocene loess deposits in the Tajik Depression, especially in the upper reaches of the Vakhsh River and Kyzylszu River, which are tributaries of the Penj River (Dodonov, 2013; Dodonov, 1991; Frechen and Dodonov, 1998). Recently, paleomagnetic results and biostratigraphic age constraints (mollusc species) indicate that loess in the Agh Band section on the NIGP commenced at ~2.4–1.8 Ma (Wang et al., 2016) (Fig. 6b), which is the oldest loess found in the northern Iran arid area. The lower Pleistocene

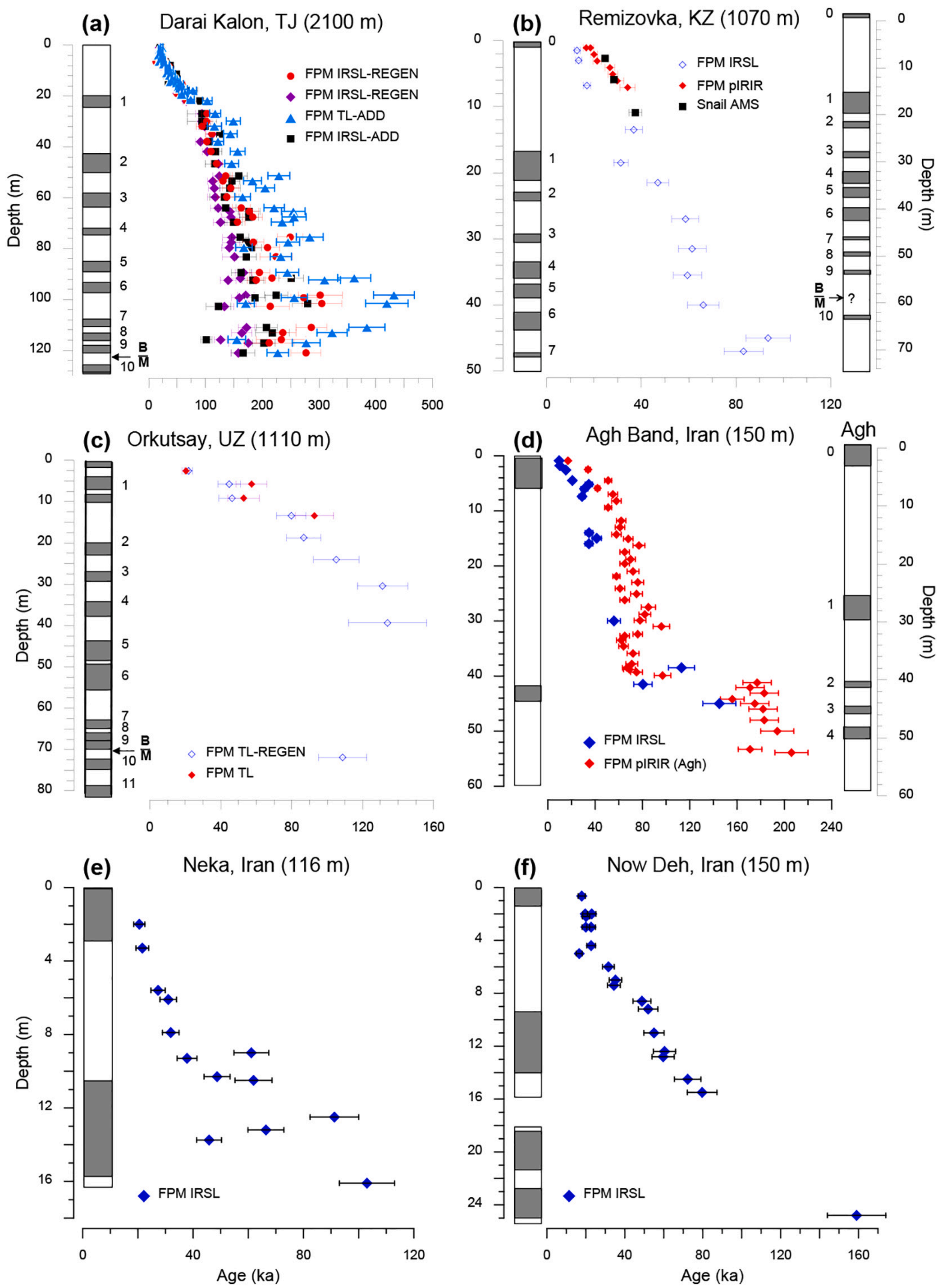

Fig. 11. Fine-grained polyminerals and K-feldspar luminescence dating of thick loess sections and comparison with their stratigraphy in Central Asia. Data sources: Dari Kalon (Frechen and Dodonov, 1998), Remizovka (Machalett et al., 2006), Okutsay (Zhou et al., 1995); Agh Band, Neka, and Now Deh (Frechen et al., 2009).

loess in Iran and south Tajikistan suggest that there was widespread loess accumulation in western Central Asia (Subregion I) during the early Pleistocene.

The Orkutsay section (Fig. 6g) in Uzbekistan contains 10 paleosol layers (PC1 ~ PC10), with a bottom age older than 0.78 Ma (B/M boundary) (Fig. 10). The stratigraphy and corresponding age in the Charvak section, which is thinner (Lazarenko et al., 1981), are similar to the Orkutsay section (Fig. 10). The loess of other sections is 40–50 m thick and overlies different geomorphic units in the Tashkent-Fergana Basin, including 3–4 weakly developed paleosol layers. The loess stratigraphy of the Orlovka section in Kyrgyzstan is >50 m thick, but the B/M boundary was not recognized in this section (Fig. 10). Loess stratigraphy in southeastern Kazakhstan is 80–100 m thick, and contains several paleosol layers. And where the preliminary estimate of the paleomagnetic age of the Remisowka section is also older than 800 ka (Fig. 9), but needs further chronological assessment (Fitzsimmons et al., 2018; Machalett et al., 2006; Machalett et al., 2008).

As stated above, the thickness of the Tianshan outcrop loess is

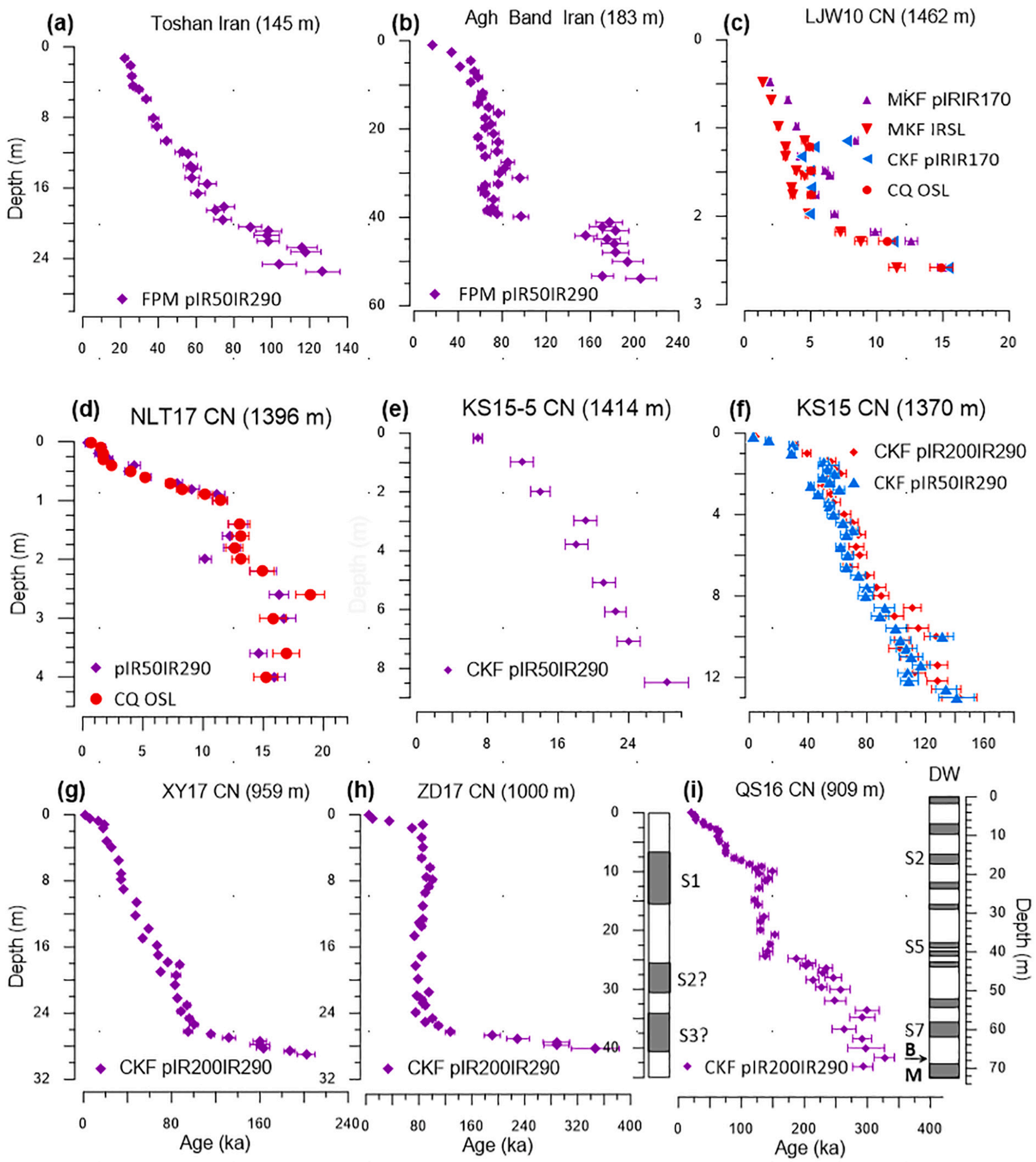

Fig. 12. Fine-grained polymineral and K-feldspar pIRIR ages with different elevated temperatures and comparison with quartz OSL ages. Data sources: Agh Band (Frechen et al., 2009); Toshan (Lauer et al., 2017a); KS15-5 (Wang et al., 2019a); XY17, NLT17 and QS16 (Li et al., 2020b); KS15 (Li et al., 2018a); LJW10 (Li et al., 2015a); ZD17(Yang et al., 2020a).

usually less than 50 m, and mainly formed during the late Quaternary (Li et al., 2015b; Song et al., 2014a). The TLD 96 m drilling core with a 0.86 Ma paleomagnetic age in the Ili Basin showed that the B/M boundary was located at L8 (Shi, 2005), similar to the Dongwan (DW) outcrop loess sediment on the northern slopes of the Tianshan (Fang et al., 2002b) and Kunlun Mountains (Fang et al., 2002a) (Fig. 10). Recently, we have drilled a 202 m core in the SGX region in the central-northern Ili Basin, and preliminary paleomagnetic results have shown that it also can reach the B/M (0.78 Ma) boundary. The KLS drilling core in the slopes of the west Kunlun Mountains near Pulu village has a much higher sedimentary rate, and the B/M boundary occurs at ~170 m (Zan et al., 2010). Parallel drilling on this site reached about 670 m, and the paleomagnetic age of 3.6 Ma (Fang et al., 2020).

Palaeomagnetic dating has great advantages in the determination of older ages, and provides a relative geochronology (age equivalence) frame of aeolian loess sediments for Quaternary climate and paleoenvironment changes. However, the absence of absolute age (e.g. tephra dating, OSL) or other supporting evidence (e.g. paleontological fossils), may result in overall chronological deviations. Furthermore, palaeomagnetic dating cannot meet the demands on required high-resolution paleoclimate reconstruction. Therefore, numeric absolute age dating methods (e.g. radiometric dating, including radiocarbon, luminescence, cosmogenic nuclides, uranium series, K/Ar, Ar/Ar) are necessary to establish reliable and accurate timescales.

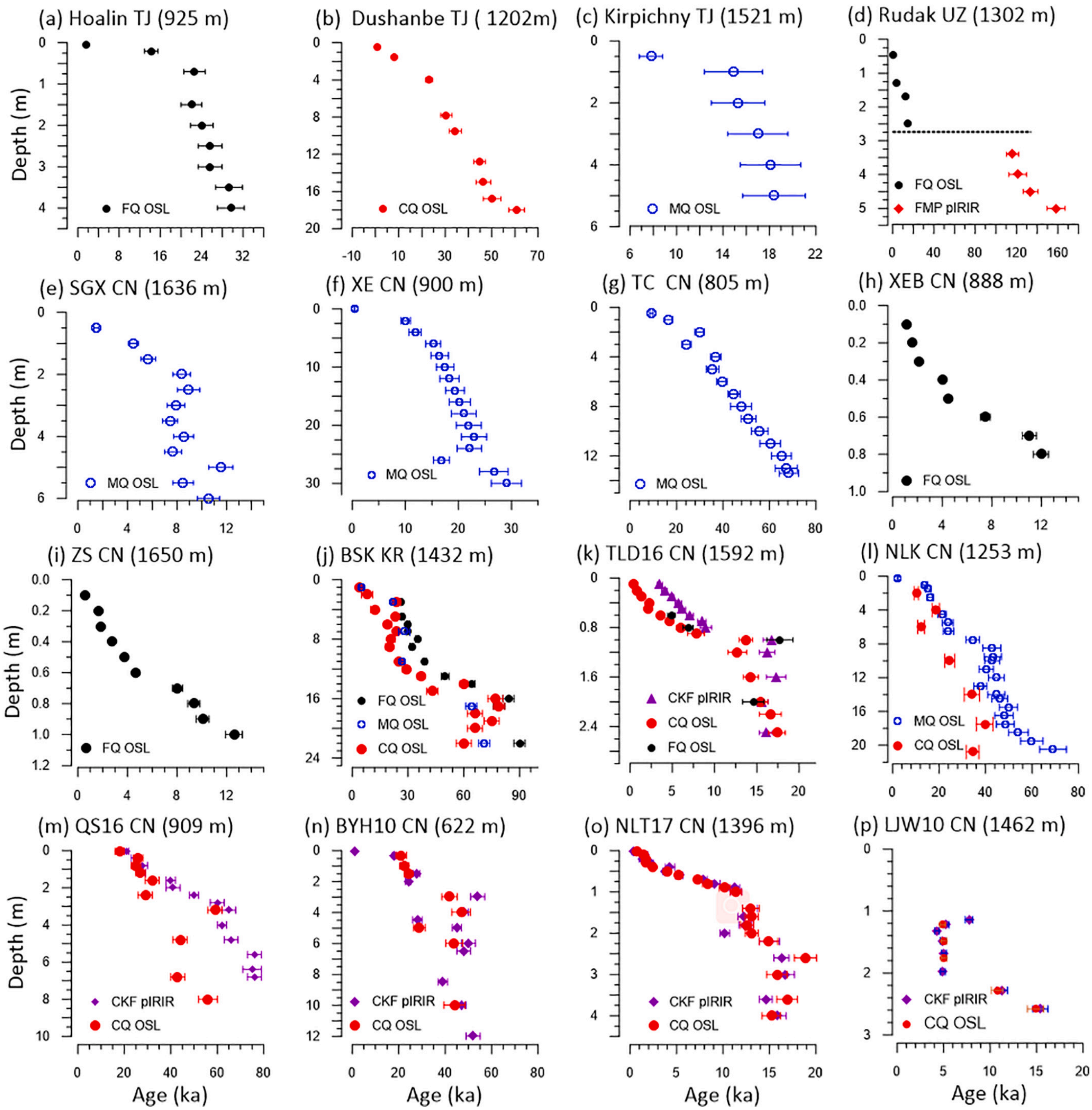

Fig. 13. Quartz OSL ages compared with K-feldspar pIRIR ages of Central Asia loess sections.Data sources: Hoalin (Wang et al., 2018); Dushanbe (Tian et al., 2021); Kirpchny (Yang et al., 2020b); Rudak (Zhang et al., 2020); SGX (Sun et al., 2020); XE (Li et al., 2016b); TC (Li et al., 2019c); XEB (Kang et al., 2020); ZS (Kang et al., 2020); BSK (Youn et al., 2014); TLD16 (Wang et al., 2019a); NLK (Song et al., 2015; Yang et al., 2014); QS16 and NLT17 (Li et al., 2020b); BYH10 (Li et al., 2016a); LJW10 (Li et al., 2015a).

4.2. Luminescence dating for Middle-Late Quaternary Central Asian loess

Luminescence dating determines the time elapsed since sediments were last exposed to sunlight and then buried in the natural environment. Luminescence dating methods include TL, IRSL and OSL. Related specific methods and their applications are not referred to in this paper, due to space constraints. Quartz and feldspar are the most used dosimeters in luminescence dating. The quartz signal (~200 Gy) saturates earlier than the feldspar signal (~2000 Gy), and theoretically, feldspars can date older samples up to 1 Ma (Buylaert et al., 2012), while quartz luminescence age is usually up to 100 ka (Lai, 2010).

TL and IRSL dating techniques have been widely applied to date Central Asian loess during the 1980s (Dodonov and Baiguzina, 1995; Frechen and Dodonov, 1998; Zhou et al., 1995). With fine-silt sized (4–11 μm) polymineral grains (FPM), the partial-bleaching TL technique yielded expected ages up to 350 ka, whereas the total-bleaching method usually yielded ages in the range of 100 to 800 ka like in Alaska and New Zealand loesses (Berger et al., 1992). Although the TL or IRSL ages showed a downward age trend with increasing depth (Fig. 11), the ages of the lowermost loess sections were much younger than the expected ages based on stratigraphic corrections and paleomagnetism. The bottom of the 120 m Darai Kalon section in the Tajikistan was dated to 300–450 ka, based on FPM TL and IRSL methods (Frechen and Dodonov, 1998) (Fig. 11a), whereas the maximum FPM IRSL age at the bottom of the Remizokvka section at 47 m depth from Kazakhstan was only 87 ka (Fig. 11b) (Machalett et al., 2006). The TL age between PC 9 and PC10 in the Orkutsay loess section from Uzbekistan, where the B/M boundary was about 0.78 Ma, was only 0.108 Ma (Fig. 11c) (Zhou et al., 1995). Due to the instabilities and difficulties with faded TL signals, Zhou et al. (1995) concluded that the FPM TL method is not reliable for CA loess dating. Significant age underestimates results from conventional FPM IRSL dating were also reported for loess sediments, which are older than 60 ka at the Agh Band section (Fig. 11d) in northern Iran, although FPM IRSL ages of loess increased with depth in the Neka section (Fig. 11e) and the Now Deh section (Fig. 11f) (Frechen et al., 2009). Fading corrections of IRSL signals should be mandatory to avoid the age underestimation.

Signal resetting prior to deposition is an important factor for the accuracy of luminescence dating. Although anomalous fading of the K-feldspar IRSL signal has precluded the reliability of this dating method, IRSL dating has several advantages over quartz OSL dating, for example a much greater signal and a wider dating range. Due to the absence of a sufficiently high preheat treatment, thermally unstable components contribute to the conventional fine-grained polymineral IRSL signals, leading to the significant age underestimation. Anomalous fading of feldspar in IRSL procedures can result in underestimation of the true age; consequently, it is essential to undertake fading experiments to correct the measured IRSL age estimates. To obtain lower fading rates and overcome anomalous fading problems, two new protocols have been developed: two-step post-IR IRSL (pIRIR) and multi-elevated-temperature post-IR IRSL (MET-pIRIR). The two-step pIRIR protocol (e.g. $pIR_{50}IR_{225}$ or $pIR_{50}IR_{290}$) utilizes an elevated temperature (e.g. 225 °C or 290 °C) IR stimulation following depletion of the signal of the low temperature IR stimulation at 50 °C (Thomsen et al., 2008) (Thiel et al., 2011). MET-pIRIR measurements can obtain a series of MET-pIRIR signals with increasing stimulation temperatures from 50 to 290 °C, thus yielding their corresponding dose values and ages (Li and Li, 2011). Stimulation at elevated temperatures significantly reduces the apparent fading rate and can produce a more stable signal compared with the conventional IRSL measured at 50 °C, which can effectively overcome the abnormal fading problem in the traditional IRSL dating process (Fitzsimmons et al., 2018). The MET-pIRIR protocol can provide reliable ages for the aeolian loess in the CLP up to ~300 ka (Li and Li, 2012) and has the potential to date samples up to ~700–800 ka in the Nihewan Basin, North China (Rui et al., 2020).

Recently, the KF pIRIR method was introduced for dating loess sediments in the Tianshan Mountains (Fig. 12). The two-step pIRIR protocol was successfully applied to the fine-grained (4–11 μm) polyminerals (FPM) fraction in the Toshan (Fig. 12a) and Agh Band (Fig. 12b) loess sections from northern Iran, and a chronostratigraphic framework since the last interglaciation has been established (Lauer et al., 2017a; Lauer et al., 2017b). Several sedimentary hiatuses of about 10 ka were identified by this method in the Agh Band section(Lauer et al., 2017b) (Fig. 12b). Li et al. (2015a) first reported that the K-feldspar pIRIR signal at a 170 °C stimulation temperature with a 200 °C preheat ($pIR_{50}IR_{170}$) can be used for both coarse-grained and medium-grained feldspar dose determinations in the LJW10 loess sections (Fig. 12c). Coarse- and medium-grained feldspar pIRIR ages are equivalent, and are also consistent with coarse quartz OSL ages, but are slightly older than MKF IRSL determined ages. Subsequently, the two step-pIRIR protocols was used for dating loess from the Ili Basin (Li et al., 2018a; Li et al., 2016a; Li et al., 2020b; Wang et al., 2019a); e.g. NLT (Fig. 12d), KS15-5 (Fig. 12e), KS15 (Fig. 12f) and at $pIR_{50}IR_{290}$, and KS15 (Fig. 12f), XY17(Fig. 12g), ZD17 (Fig. 12 h) and QS16 (Fig. 12i) at $pIR_{200}IR_{290}$. Comparison between the $pIR_{200}IR_{290}$ and $pIR_{50}IR_{290}$ ages in the KS15 section from the Ili Basin indicated equivalent ages, although it appears that $pIR_{200}IR_{290}$ ages are slightly older than $pIR_{50}IR_{290}$ ages (Fig. 12e). The CKF pIRIR ages are consistent with CQ OSL ages, within the acceptable uncertainty range, in the NLT17 section (Fig. 12h) from the Ili Basin (Li et al., 2020b). A MET-pIRIR dating using low temperatures (i.e., 110, 140, and 170 °C) was introduced to determine the De values for the K-feldspar grains to date two Holocene loess sections in the northern piedmont of Tianshan Mountains(Zhao et al., 2015). The ages in both sections are in good stratigraphic order, and ae consistent with their quartz OSL SAR ages. The above results indicate that both pIRIR and OSL dating methods can obtain reliable ages within the most recent glacial period, and are supported by proxies and paleoclimate reconstruction (Li et al., 2018a; Li et al., 2020b; Wang et al., 2019a). The CKF pIRIR dating method is suitable up to 320 ka in the QS16 loess section (Fig. 12i) from the northern slopes of the Tianshan Mountains (Li et al., 2020b) and even to 347 ka in the ZD17 section (Fig. 12h) in the Ili Basin. Because no obvious paleosol layer was observed in the field, they assumed that the stratigraphy between depths from 34 m to 41 m is equivalent to S3 (about 300–340 ka) in the Chinese Loess Plateau on the base of pIRIR ages; however, the stratigraphy around 40 m depth of the adjacent Dongwan (DW) loess section (Fang et al., 2002b) (Fig. 10) in the same loess ridge is similar to S5 (about 500–580 ka) based on paleomagnetic age, which is much older than that of QS16 section. We wonder if the pIRIR ages of the QS16 section were underestimated. Relative to conventional IRSL, and pIRIR methods have extended the age-limitation; however, more work is required to improve the reliability for older samples beyond the last glacial–interglacial period.

Since 2000, OSL dating has been widely applied to determine the chronology of late Quaternary loess. Many researchers have used quartz of different grain sizes for OSL dating in CA, including fine -grained (4–11 μm) quartz (FQ) (Feng et al., 2011; Kang et al., 2020; Kang et al., 2015b; Lu et al., 2016; Song et al., 2012; Wang et al., 2018), medium -grained (38–63 μm) quartz (MQ) (Duan et al., 2020; E et al., 2012; Li et al., 2016b; Li et al., 2019c; Song et al., 2015; Yang et al., 2020b), and coarse -grained (63–90–250 μm) quartz (CQ) (Li et al., 2015a; Tian et al., 2021; Wang et al., 2019b; Yang et al., 2014; Youn et al., 2014). Generally, the quartz OSL ages indicate a downward age trend with increasing depth, up to 80 ka (Fig. 13a–i). The CQ OSL ages are slightly younger than the FQ OSL ages of the BSK loess section (Fig. 13j) in the Chu River Basin (Youn et al., 2014)and the TLD16 loess section (Fig. 13k) in the Ili Basin (Wang et al., 2019a). The CQ OSL ages are also younger than the MQ OSL ages of the NLK loess section (Fig. 13l) in the Ili Basin (Song et al., 2015; Yang et al., 2014). Furthermore, when samples are older than 40 ka, the CQ OSL ages appear out of order and even reversed: e.g. BSK, NLK, QS16 (Fig. 13m), and BYH10 (Fig. 13n). Youn et al. (2014) argued that the OSL ages of fine and coarse quartz fractions in the Bishkek (BSK) loess section are consistent with each other within 2σ error (Youn et al., 2014), although differences are observed (Fig. 13j). These discrepancies were probably caused by the high over-dispersion of the coarse-grained quartz and an early saturation of the quartz OSL signal (Li et al., 2020b). Therefore, more investigation is needed to verify which grain size of quartz is most reliable for OSL dating of CA loess.

It is worth noting that the CQ OSL ages are generally consistent with the coarse-grained K-feldspar (CKF) pIRIR ages, when the samples are less than 40 ka, e.g. QS16 (Fig. 13m), BYH10 (Fig. 13n) (Li et al., 2016a), NLT17 (Fig. 13o) (Li et al., 2020b). Low OSL signal intensities of the coarse-grained quartz or incomplete bleaching might result in a high over-dispersion dose distribution and even age reversals, but the exact reason for this underestimation is still unclear and needs further study. Therefore, Li et al. (2016a) suggested that coarse quartz OSL ages less than 40 ka and K-feldspar pIRIR ages up to 150 ka are reliable for loess samples (Li et al., 2016a; Li et al., 2020b). The fine-grained quartz OSL dating of well-bleached loess sediments can produce reliable ages up to 60–80 ka, e.g. the TC and BSK sections (Fig. 13).

4.3. Radiocarbon dating of the last glacial and Holocene Central Asian loess

Radiocarbon dating methods are widely used for determining the age of various types of carbon-containing materials, with an upper age limit of about 50–60 ka. Charcoal is an ideal material for determining reliable radiocarbon age. Although there are some microcharcoals found in Central Asian loess (Miao et al., 2020; Wu et al., 2020), their abundance is not usually sufficient for radiocarbon dating, which greatly restricts application of the AMS ^{14}C dating method for CA loess. Widespread terrestrial snails, mainly *Cathaica rossimontana* and *Wlirus spp,* in Central Asian loess sediments (Zong et al., 2020) provide an alternative material for radiocarbon dating. Radiocarbon ages are usually based on total organic carbon (TOC)/soil organic matter (SOM) of bulk sediments (Han et al., 2019; Shu et al., 2018; Song et al., 2015; Song et al., 2012; Song et al., 2018b), or snail shells (Duan et al., 2020; Feng et al., 2011) (Fig. 14). The oldest radiocarbon age previously reported based on snail shells was about 46 ka, (Feng et al., 2011), and most AMS ^{14}C ages of TOC in loess sediments from CA are younger than 40 ka. Snail shell

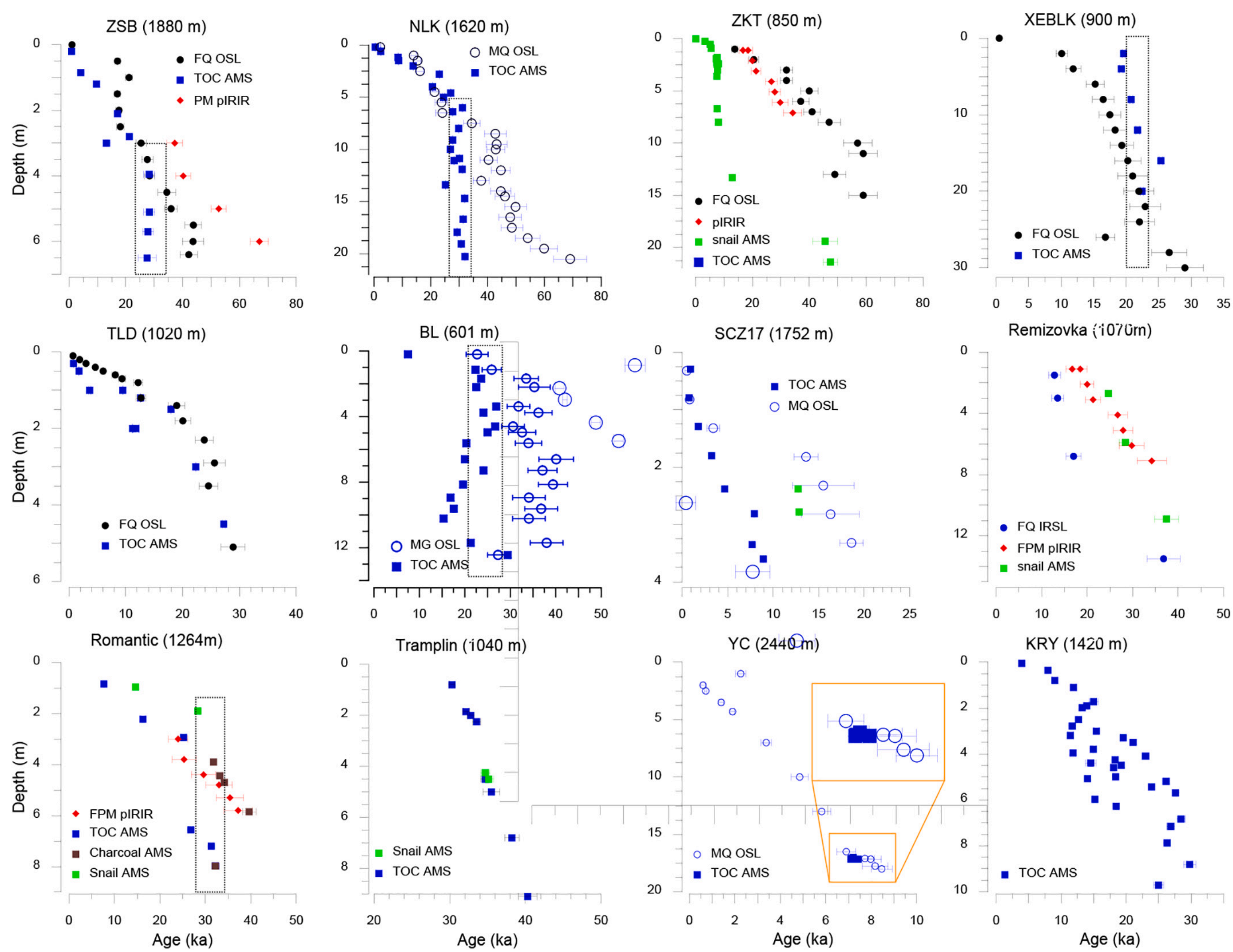

Fig. 14. Comparison between radiocarbon and luminescence ages of loess sections in Central Asia.
Data sources: ZSB (Song et al., 2012; Song et al., 2018a); NLK (Song et al., 2015; Yang et al., 2014); XEBLK (Cheng et al., 2020b; Li et al., 2016b); TLD (Kang et al., 2015b; Zong et al., 2020); SCZ17 (Duan et al., 2020); Remizovka (Fitzsimmons et al., 2018; Machalett et al., 2006); Romantic and Tramplin (Feng et al., 2011); Mailbulak (Fitzsimmons et al., 2018); YC (Han et al., 2019); KRY (Shu et al., 2018).
Minerals: Q: quartz; KF- potassium feldspar; PM: polyminerals.
Grain size: F: fine-grained (4-11 μm); M: medium-grained (38-63 μm); C: coarse-grained (63–90–250 μm).

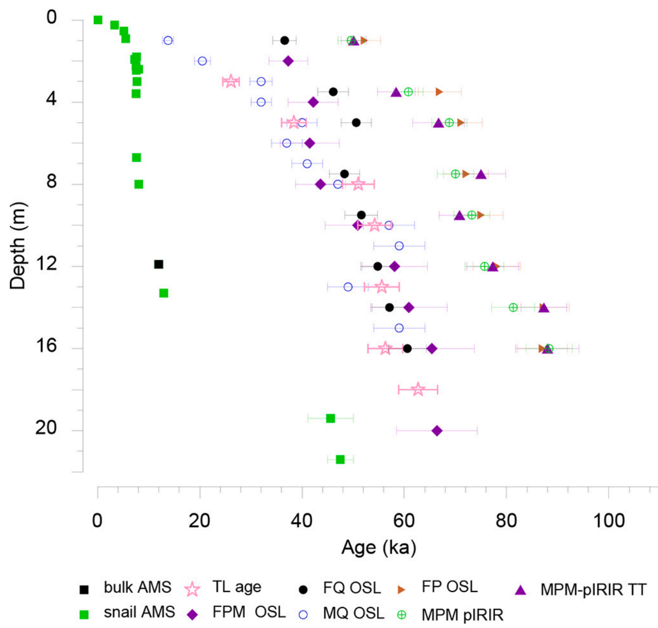

Fig. 15. Dating ages of the Zeketai loess section based on different dating techniques.
Data from the references (E et al., 2012; Feng et al., 2011; Qin and Zhou, 2018). MP: medium-grained polymineral; FP: fine-grained polymineral; FQ: fine-grained quartz; TT corrected: the $pIRIR_{225}$ ages with the correction of the thermal transferred (TT) -$pIRIR_{225}$ signal.

radiocarbon ages are older than TOC or bulk sediments ages determined in SCZ17, and from the Romantic section; except for the ZKT section, the snail AMS ^{14}C are equivalent to OSL ages within the acceptable error ranges.

Comparison between AMS ^{14}C and OSL ages in the Ili Basin (Fig. 14) has shown that both quartz OSL and AMS ^{14}C ages of TOC/SOM are generally consistent with the stratigraphic sequence when the sample ages are younger than 25 ka, which means that both procedures can be used to establish a reliable chronology in the Ili Basin. However, the AMS^{14}C ages beyond 30 ka are complicated and irregular, and are often younger than the OSL ages (Fig. 14) (Song et al., 2015; Song et al., 2012; Song et al., 2018a; Zhang et al., 2020). Such discrepancy between OSL and radiocarbon ages of loess samples was also reported in BL and SCZ17 loess sections from the northern slopes of the Tianshan Mountains (Duan et al., 2020) and the Bishkek loess section in the western Tianshan Mountains (Youn et al., 2014). The underestimation of radiocarbon ages may be attributed to carbon contamination induced by organic matter from secondary pedogenic carbonate, chemical alternation, translocation of soluble organic matter and/or bioturbation (E et al., 2012; Song et al., 2015; Song et al., 2012; Song et al., 2018a). However, the differences between radiocarbon and OSL ages of loess sections from the northern slopes of the western Tianshan Mountains (e. g. Remizovka, Romantic, Tramplin sections) (Feng et al., 2011) (Fitzsimmons et al., 2018; Machalett et al., 2006), and the YC section (Han et al., 2019) in the south margin of the Tarim Basin, are not obvious. Dating results of some sections indicate that the radiocarbon ages do not show increments (e.g. ZSB, NLK, Romantic, and KRY), or even reverse (e.g. BL KRY) with increasing depths (Fig. 14).

There is no consensus on the reliability and precision of the various dating methods for CA loesses. For example, although many researchers have investigated the Zeketai (ZKT) loess (Fig. 15), which was considered in the 1980s as important loess sediment in Xinjiang, similar to the Luochuan loess section in the CLP, the ages are still under debate. From the consideration of models based on the ages of bulk sediment, charcoal and snails, Feng et al. (2011) argued that the luminescence dating method was not reliable, due to the loess TL and OSL clocks in the ZKT section were incompletely zeroed or bleached when loess deposition originated primarily from local riverbeds. Consequently, the quartz OSL ages were overestimated, and hence the radiocarbon ages were more reliable. However, E et al. (2012) compared the MQ OSL dating results of the Zeketai section with those of the previous FQ OSL dating (Feng et al., 2011) and found good consistency between them (Fig. 15), thus concluding that the OSL dating procedure was reliable. A recent parallel study of OSL and pIRIR on different quartz grains and polyminerals indicated that the FQ OSL ages were in stratigraphic order and ranged from 37 ka to 61 ka, but were ~30% younger than the FPM and MPM MET pIRIR ages (Qin and Zhou, 2018) (Fig. 15). The authors argued that the quartz OSL ages of this loess section were likely to be underestimated, especially for samples older than 40 ka, and they recommended in applying the polyminerals, or K-feldspar pIRIR signals for dating loess in the Ili Basin.

In summary, AMS ^{14}C of loess sediments can obtained reliable age up to 25 ka, caution should be exercised for AMS ^{14}C ages older than 25 ka. OSL dating of quartz with different particle sizes provides accurate dates of loess deposits, especially since MIS3, although the upper limit of quartz OSL dating is not uniform. K-feldspar pIRIR and two steps-pIRIR dating methods have a wide range of potential dating up to 250 ka in arid Central Asia, although the procedure may overestimate the age of younger sediments. However, the complicated topography, proximal loess deposition and local climate condition differentiation, as well as other factors, such as dating material availability, carbon contamination, the reliability of luminescence signals, in -situ depositional processes and the complexity of remanence acquisition, may have significant impacts on the inferred chronology in CA loess. Therefore, caution is still essential for paleoclimate and paleoenvironmental reconstruction when using any single chronological model, and therefore additional studies are required to achieve a comprehensive, reliable geochronological sequence. Relative dating approaches, such as amino acid geochronology (Machalett et al., 2008) and relative paleomagnetic intensity (RPI) (Li et al., 2020a), offer an independent assessment of numerical age estimates, when results are at or near their methodological limits, and can assist in the chronostratigraphic evaluation of loess units beyond the range of useful numerical dating methods.

4.4. Spatial-temporal distributions of Central Asian loess ages and their implications for dust sedimentation

Although there is some debate and inconsistency regarding the reliability of CA loess ages, we have found that the dust sedimentary processes differ to some extent from those in the CLP. There are three obvious characteristics, as follows. 1) Rapid accumulations: both OSL and AMS ^{14}C dating of several sections indicates that ages are clustered or even inverse at some depths, implying extremely high sedimentation rates(Li et al., 2020b; Li et al., 2016b; Sun et al., 2020). 2) Discontinuity or sedimentary hiatus. These non-conformities are often hard to detect by untrained observers, but obvious age gaps can be observed in age statistics (Fig. 16) and depth-age plots, e.g. the Agh Band section, Now Deh section (Frechen et al., 2009), Kalat-e Naderi section(Karimi et al., 2011) in the Caspian Lowland of northern Iran, and the Rudak loess section in Uzbekistan (Zhang et al., 2020). 3) The upper Holocene sediments, especially in Subregion I (Fig. 16), are frequently omitted, based on statistics of age results (See Supplementary Table 2). Their absence may be caused by an arid climate and wind/fluvial erosion.

Frequency distributions of luminescence ages have been used to evaluate dust accumulation/activity intensity (Kang et al., 2015a; Ling et al., 2020; Singhvi et al., 2001; Yu and Lai, 2012) under the same exposure conditions with regular sampling intervals. To extract dust accumulation from the array of luminescence ages, we collected all luminescence ages of loess samples from CA (Fig. 16), regardless to dating materials and methods, accuracies and sampling intervals. Frequency statistics were based on 1281 luminescence ages (See Supplementary Table 3) at 1 kyr, 2 kyr, 5 kyr intervals for the periods of 0–80

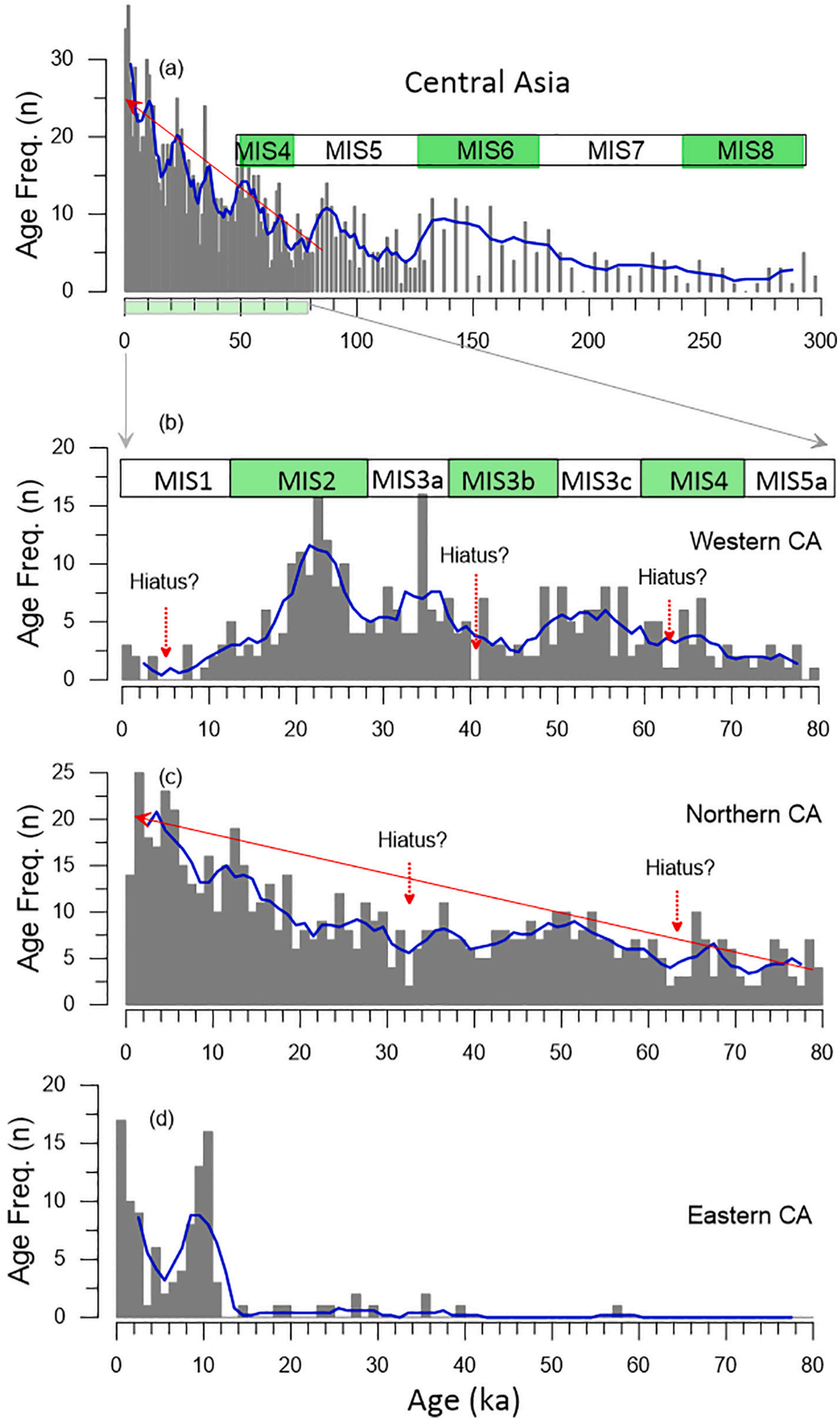

Fig. 16. Spatial and temporal distribution of loess luminescence ages in Central Asia.

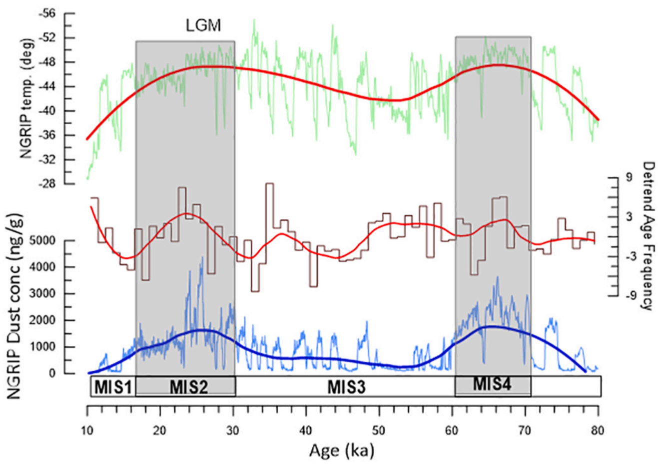

Fig. 17. Comparison between detrended fluctuation of age frequencies in Central Asia with NGRIP temperature (Karimi et al., 2011) and dust concentrations (Steffensen, 1997).

ka, 80–130 ka and 130–300 ka, respectively. The total luminescence age frequency distribution curve (Fig. 16a) indicates two obvious peaks during the cold MIS6 and MIS4 periods, although the trend of ages frequencies increases quickly since the last glacial period, which may be due to the sampling strategy and/or the section thicknesses. Because the reliability of luminescence ages beyond 80 ka still requires further assessment, we have focused on the ages since the last glacial period. Obviously different patterns are observed in the three subregions (Fig. 16b–d). The age frequency curve reveals three clusters in western CA (Fig. 16b) during the last glacial period, and two clusters in eastern CA during the Holocene (Fig. 16d), while there are no obvious peaks in northern CA (Fig. 16d). In order to exclude the possible effects of sampling densities, we detrended the age frequencies, and compared them with NGRIP temperature and dust concentrations (Fig. 17). It was found that the intervals with higher age frequencies roughly correspond to high NGRIP dust concentrations during cold glacial periods, especially for the last maximum glacial (MIS2), but there was no obvious relationship during interglacials. This suggest that the cold glacial periods are liable to promote dust activities. These spatial and temporal differences imply varying dust activities at glacial-interglacial orbital timescale.

To explore the dust activities/events, these luminescence ages were plotted using a probability density function (PDF). An age cluster in a PDF plot can be interpreted either as a higher and accidental sampling density of sediments belonging to a specific interval and/or as a reflection of enhanced dust accumulation/activities(Kang et al., 2015a; Singhvi et al., 2001; Yu and Lai, 2012). Several similar age clusters around 12 ka, 22–28 ka, 35–36 ka, 66 ka were observed in the three subregions (Fig. 18), which may suggest that strong dust activities on a millennial-scale are synchronous in Central Asia. However, the probability densities of several events are not similar, where some local dust events need to be considered. These disparities imply different strengths of controlling factors and the effects of regional conditions, e.g. climate, landform and vegetation may occur. Ideally, the PDF plots based on the same dating methods and regular sampling intervals should be more significant for paleoclimate interpretation.

5. Conclusions

This paper presents a systematic investigation of the distribution, thickness, ages, and continuity of loess or loess-like sediments in CA and their implications. Loess sediments are mainly distributed on the windward piedmonts of Central Asian high mountains and river terraces, and present distinct pedogenic characteristics. Taking into consideration the disparities of loess-paleosol composition, climate differences and topographic effects, we divided the loess distribution in CA into three subregions, namely Western CA (Subregion I), Northern CA (Subregion II), and Eastern CA (Subregion III). The subregions were roughly consistent with the 60% and 30% winter-half year's precipitation percentage contours, and also corresponded to three loess depocenters with thicknesses greater than 200 m. Subregion I was characterized by obvious loess-paleosol couplets, which was analogous to those of the CLP. Subregion II had uncertain pedogenesis depending on the altitude or precipitation; Subregion III had no obvious pedogenesis sandy loess.

Previous chronostratigraphic data of CA loess and our field investigations indicated that most of loess outcrops have developed since

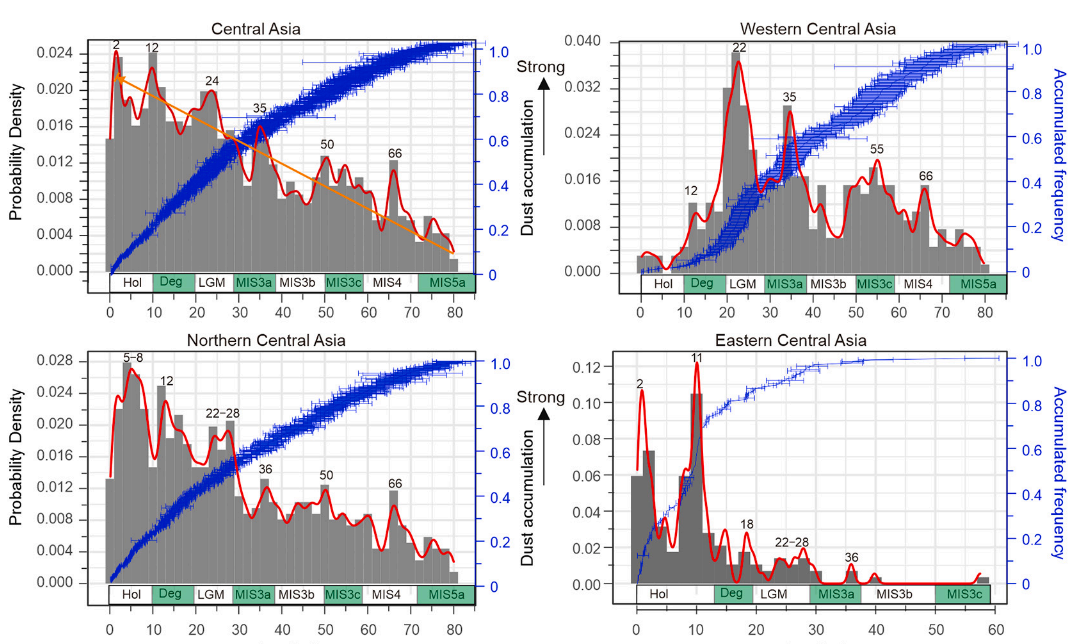

Fig. 18. Probability density functions (PDFs) of loess sediment ages in different regions of Central Asia.

the last interglacial-glacial period, although CA loess sediments can span the entire Quaternary period, and even can extend to the Pliocene periods. AMS ^{14}C can provide reliable ages for the last 25–30 kyr. Both Quartz OSL and K-feldspar pIRIR dating techniques based on well-bleached natural environmental materials can provide reliable ages for younger samples, less than 80–100 ka. Dating of deposits at elevated locations shows that CA loess deposits at some locations are rapid and discontinuous, which requires caution in the interpretation of proxies and paleoenvironment. Spatial-temporal distributions of CA loess luminescence ages indicated that there are different clusters in different loess subregions, but generally, the strong dust activities occurred during cold glacial periods or stadials. New dating techniques should be developed in future research to meet the high-resolution paleoclimate reconstruction in CA and around the world.

Supplementary data to this article can be found online at https://doi.org/10.1016/j.palaeo.2021.110279.

Declaration of Competing Interest

The authors declare that they have no known competing financial interests or personal relationships that could have appeared to influence the work reported in this paper.

Acknowledgements

This study was supported by the Natural Science Foundation of China (Nos: 41977385, 41572162) and the Second Tibetan Plateau Scientific Expedition and Research program (No: 2019QZKK0101). This study is also funded by the and State Key Laboratory of Loess and Quaternary Geology (No: SKLLQGPY2006) and the International Partnership Program of the Chinese Academy of Sciences. Many thanks to Prof. Yaoming Li, Prof. Xi Chen from the Research Center for Ecology and Environment of Central Asia, Liancheng Tan, Yanjun Cai, Xiaoke Qiang, Zhangdong Jin, Xulong Wang, Qiang Li, Dong Li, Junchao Dong from IEECAS for their assistances in Central Asia field campaigns. We thank Dr. Xin Wang for providing photos of the Iran AB section. We appreciate Chief-in-Editor Prof. Thomas Algeo, Guest Editor Prof. Chunhui Song and two anonymous reviewers for their critical comments and valuable suggestions. We also thank Andrew Mackie for language editing.

References

Aizen, V., Aizen, E., 1997. Hydrological cycles on the north and south peripheries of mountain–glacial basins of Central Asia. Hydrol. Process. 11 (5), 451–469. https://doi.org/10.1002/(SICI)1099-1085(199704)11:5<451::AID-HYP448>3.0.CO;2-M.

Aizen, V.B., Aizen, E.M., Melack, J.M., 1996. Precipitation, melt and runoff in the northern Tien Shan. J. Hydrol. 186 (1–4), 229–251. https://doi.org/10.1016/S0022-1694(96)03022-3.

Aizen, V.B., Aizen, E.M., Joswiak, D.R., Fujita, K., Takeuchi, N., Nikitin, S.A., 2006. Climatic and atmospheric circulation pattern variability from ice-core isotope/geochemistry records (Altai, Tien Shan and Tibet). Ann. Glaciol. 43 (1), 49–60. https://doi.org/10.3189/172756406781812078.

An, Z., Kukla, G.J., Porter, S.C., Xiao, J., 1991. Magnetic susceptibility evidence of monsoon variation on the Loess Plateau of central China during the last 130,000 years. Quat. Res. 36 (1), 29–36. https://doi.org/10.1016/0033-5894(91)90015-W.

Asadi, S., Moore, F., Keshavarzi, B., 2013. The nature and provenance of Golestan loess deposits in northeast Iran. Geol. J. 48 (6), 646–660. https://doi.org/10.1002/gj.2466.

Berger, G.W., Pillans, B.J., Palmer, A.S., 1992. Dating loess up to 800-Ka by thermoluminescence. Geology 20 (5), 403–406. https://doi.org/10.1130/0091-7613(1992)020<0403:DLUTKB>2.3.CO;2.

Buylaert, J.-P., Jain, M., Murray, A.S., Thomsen, K.J., Thiel, C., Sohbati, R., 2012. A robust feldspar luminescence dating method for Middle and Late Pleistocene sediments. Boreas 41 (3), 435–451. https://doi.org/10.1111/j.1502-3885.2012.00248.x.

Cai, Y.J., Chiang, J.C.H., Breitenbach, S.F.M., Tan, L.C., Cheng, H., Edwards, R.L., An, Z. S., 2017. Holocene moisture changes in western China, Central Asia, inferred from stalagmites. Quat. Sci. Rev. 158, 15–28. https://doi.org/10.1016/j.quascirev.2016.12.014.

Chen, Q., Liu, X., Heller, F., Hirt, A.M., Lü, B., Guo, X., Mao, X., Chen, J., Zhao, G., Feng, H., 2012. Susceptibility variations of multiple origins of loess from the Ily Basin (NW China). Chin. Sci. Bull. 57 (15), 1844–1855. https://doi.org/10.1007/s11434-012-5131-1.

Chen, F., Chen, J., Huang, W., Chen, S., Huang, X., Jin, L., Jia, J., Zhang, X., An, C., Zhang, J., Zhao, Y., Zicheng, Y., Zhang, R., Liu, J., Zhou, A., Feng, S., 2019. Westerlies Asia and monsoonal Asia: Spatiotemporal differences in climate change and possible mechanisms on decadal to suborbital timescales. Earth-Sci. Rev. 192, 337–354. https://doi.org/10.1016/j.earscirev.2019.03.005.

Chen, X., Song, Y., Li, Y., Huang, Y., Zhou, X., Fan, Y., 2021. Provenance of sub-aerial surface sediments in the Tarim Basin, Western China. Catena 198, 105014. https://doi.org/10.1016/j.catena.2020.105014.

Cheng, H., Zhang, P.Z., Spötl, C., Edwards, R.L., Cai, Y.J., Zhang, D.Z., Sang, W.C., Tan, M., An, Z.S., 2012. The climatic cyclicity in semiarid-arid central Asia over the past 500,000 years. Geophys. Res. Lett. 39 (1), 1705. https://doi.org/10.1029/2011GL050202.

Cheng, L., Song, Y., Sun, H., Bradák, B., Orozbaev, R., Zong, X., Liu, H., 2020a. Pronounced changes in paleo-wind direction and dust sources during MIS3b recorded in the Tacheng loess, northwest China. Quat. Int. 552, 122–134. https://doi.org/10.1016/j.quaint.2019.05.002.

Cheng, L.Q., Song, Y.G., Chang, H., Li, Y., Orozbaev, R., Zeng, M.X., Liu, H.F., 2020b. Heavy mineral assemblages and sedimentation rates of eastern Central Asian loess: Paleoenvironmental implications. Palaeogeogr. Palaeoclimatol. Palaeoecol. 551, 109747. https://doi.org/10.1016/j.palaeo.2020.109747.

Ding, Z.L., Derbyshire, E., Yang, S.L., Yu, Z.W., Xiong, S.F., Liu, T.S., 2002a. Stacked 2.6-Ma grain size record from the Chinese loess based on five sections and correlation with the deep-sea δ18O record. Paleoceanography 17 (3). https://doi.org/10.1029/2001PA000725, 5-1-5-21.

Ding, Z.L., Ranov, V., Yang, S.L., Finaev, A., Han, J.M., Wang, G.A., 2002b. The loess record in southern Tajikistan and correlation with Chinese loess. Earth Planet. Sci. Lett. 200, 387–400. https://doi.org/10.1016/S0012-821X(02)00637-4.

Ding, Z., Derbyshire, E., Yang, S., Sun, J., Liu, T., 2005. Stepwise expansion of desert environment across northern China in the past 3.5 Ma and implications for monsoon evolution. *Earth Planet. Sci.* Lett. 237 (1–2), 45–55. https://doi.org/10.1016/j.epsl.2005.06.036.

Dodonov, A.E., 1991. Loess of central Asia. Geojournal 24 (2), 185–194.

Dodonov, A., 2013. Loess records| central Asia. In: Elias Scott, M.J.C. (Ed.), Encyclopedia of Quaternary Science. Elsevier, AMSTERDAM, pp. 1418–1429.

Dodonov, A.E., Baiguzina, L.L., 1995. Loess stratigraphy of Central Asia: Palaeoclimatic and palaeoenvironmental aspects. Quat. Sci. Rev. 14 (7–8), 707–720. https://doi.org/10.1016/0277-3791(95)00054-2.

Dodonov, A., Penkov, A., 1977. Some data on the stratigraphy of the watershed loesses in the Tajik depression. J. Bull. Comm. Quat. Res. 47, 67–76.

Dodonov, A.E., Shackleton, N., Zhou, L.P., Lomov, S.P., Finaev, A.F., 1999. Quaternary loess-paleosol stratigraphy of Central Asia: Geochronology, correlation, and evolution of paleoenvironments. Stratigr. Geol. Correl. 7 (6), 581–593.

Dodonov, A.E., Sadchikova, T.A., Sedov, S.N., Simakova, A.N., Zhou, L.P., 2006. Multidisciplinary approach for paleoenvironmental reconstruction in loess-paleosol studies of the Darai Kalon section, Southern Tajikistan. Quat. Int. 152-153, 48–58. https://doi.org/10.1016/j.quaint.2005.12.001.

Duan, F., An, C., Wang, W., Herzschuh, U., Zhang, M., Zhang, H., Liu, Y., Zhao, Y., Li, G., 2020. Dating of a late Quaternary loess section from the northern slope of the Tianshan Mountains (Xinjiang, China) and its paleoenvironmental significance. Quat. Int. 544, 104–112. https://doi.org/10.1016/j.quaint.2020.02.034.

E, C.Y., Lai, Z.P., Sun, Y.J., Hou, G.L., Yu, L.P., Wu, C.Y., 2012. A luminescence dating study of loess deposits from the Yili River basin in western China. Quat. Geochronol. 10, 50–55. https://doi.org/10.1016/j.quageo.2012.04.022.

Evans, M., Heller, F., 1994. Magnetic enhancement and palaeoclimate: study of a loess/palaeosol couplet across the Loess Plateau of China. Geophys. J. Int. 117 (1), 257–264.

Fang, X., Lu, L.Q., Yang, S.L., Li, J.J., An, Z.S., Jiang, P., Chen, X.L., 2002a. Loess in Kunlun Mountains and its implications on desert development and Tibetan Plateau uplift in west China. Sci. China Ser. D. 45 (4), 289–299.

Fang, X.M., Shi, Z.T., Yang, S.L., Yan, M.D., Li, J.J., Jiang, P.A., 2002b. Loess in the Tian Shan and its implications for the development of the Gurbantunggut Desert and drying of northern Xinjiang. Chin. Sci. Bull. 47 (6), 1381–1387.

Fang, X., An, Z., Clemens, S.C., Zan, J., Shi, Z., Yang, S., Han, W., 2020. The 3.6-Ma aridity and westerlies history over midlatitude Asia linked with global climatic cooling. Proc. Natl. Acad. Sci. https://doi.org/10.1073/pnas.1922710117.

Feng, Z.D., Ran, M., Yang, Q.L., Zhai, X.W., Wang, W., Zhang, X.S., Huang, C.Q., 2011. Stratigraphies and chronologies of late Quaternary loess–paleosol sequences in the core area of the central Asian arid zone. Quat. Int. 240 (1–2), 156–166. https://doi.org/10.1016/j.quaint.2010.10.019.

Fitzsimmons, K.E., Sprafke, T., Zielhofer, C., Günter, C., Deom, J.-M., Sala, R., Iovita, R., 2018. Loess accumulation in the Tian Shan piedmont: Implications for palaeoenvironmental change in arid Central Asia. Quat. Int. 469, 30–43. https://doi.org/10.1016/j.quaint.2016.07.041.

Fitzsimmons, K.E., Nowatzki, M., Dave, A.K., Harder, H., 2020. Intersections between wind regimes, topography and sediment supply: Perspectives from aeolian landforms in Central Asia. Palaeogeogr. Palaeoclimatol. Palaeoecol. 540, 109531. https://doi.org/10.1016/j.palaeo.2019.109531.

Forster, T., Heller, F., 1994. Loess deposits from the Tajik Depression (Central-Asia) - magnetic-properties and paleoclimate. Earth Planet. Sci. Lett. 128 (3–4), 501–512.

Frechen, M., Dodonov, A.E., 1998. Loess chronology of the middle and upper Pleistocene in Tadjikistan. Geol. Rundsch. 87 (1), 2–20. https://doi.org/10.1007/s005310050185.

Frechen, M., Kehl, M., Rolf, C., Sarvati, R., Skowronek, A., 2009. Loess chronology of the Caspian Lowland in Northern Iran. Quat. Int. 198 (1–2), 220–233. https://doi.org/10.1016/j.quaint.2008.12.012.
Ghafarpour, A., Khormali, F., Balsam, W., Karimi, A., Ayoubi, S., 2016. Climatic interpretation of loess-paleosol sequences at Mobarakabad and Aghband, Northern Iran. Quat. Res. 86 (1), 95–109. https://doi.org/10.1016/j.yqres.2016.05.004.
Gong, D.Y., Ho, C.H., 2002. The Siberian High and climate change over middle to high latitude Asia. Theor. Appl. Climatol. 72 (1–2), 1–9.
Groll, M., Opp, C., Aslanov, I., 2013. Spatial and temporal distribution of the dust deposition in Central Asia – results from a long term monitoring program. Aeolian Res. 9, 49–62. https://doi.org/10.1016/j.aeolia.2012.08.002.
Guo, Z.T., Ruddiman, W.F., Hao, Q.Z., Wu, H.B., Qiao, Y.S., Zhu, R.X., Peng, S.Z., Wei, J. J., Yuan, B.Y., Liu, T.S., 2002. Onset of Asian desertification by 22 Myr ago inferred from loess deposits in China. Nature 416, 159–163. https://doi.org/10.1038/416159a.
Han, W.X., Lu, S., Appel, E., Berger, A., Madsen, D., Vandenberghe, J., Yu, L.P., Han, Y. X., Yang, Y.B., Zhang, T., Teng, X.H., Fang, X.M., 2019. Dust storm outbreak in Central Asia After similar to 3.5 kyr BP. Geophys. Res. Lett. 46 (13), 7624–7633. https://doi.org/10.1029/2018gl081795.
Hao, Q., Wang, L., Oldfield, F., Peng, S., Qin, L., Song, Y., Xu, B., Qiao, Y., Bloemendal, J., Guo, Z., 2012. Delayed build-up of Arctic ice sheets during 400,000-year minima in insolation variability. Nature 490 (7420), 393–396. https://doi.org/10.1038/nature11493.
Heller, F., Evans, M.E., 1995. Loess magnetism. Rev. Geophys. 33 (2), 211–240. https://doi.org/10.1029/95RG00579.
Heller, F., Liu, T.S., 1982. Magnetostratigraphical dating of loess deposits in China. Nature 300 (5891), 431–433. https://doi.org/10.1038/300431a0.
Heller, F., Liu, T., 1986. Palaeoclimatic and sedimentary history from magnetic susceptibility of loess in China. Geophys. Res. Lett. 13 (11), 1169–1172.
Heller, F., Shen, C.D., Beer, J., Liu, X.M., Liu, T.S., Bronger, A., Suter, M., Bonani, G., 1993. Quantitative estimates of pedogenic ferromagnetic mineral formation in Chinese Loess and paleoclimatic implications. Earth Planet. Sci. Lett. 114 (2–3), 385–390. https://doi.org/10.1016/0012-821x(93)90038-B.
Huang, W., Chen, J.H., Zhang, X.J., Feng, S., Chen, F.H., 2015. Definition of the core zone of the "westerlies-dominated climatic regime", and its controlling factors during the instrumental period. Sci. China-Earth Sci. 58 (5), 676–684. https://doi.org/10.1007/s11430-015-5057-y.
Indoitu, R., Orlovsky, L., Orlovsky, N., 2012. Dust storms in Central Asia: spatial and temporal variations. J. Arid Environ. 85, 62–70. https://doi.org/10.1016/j.jaridenv.2012.03.018.
Jia, J., Xia, D., Wang, B., Wei, H., Liu, X., 2012. Magnetic investigation of Late Quaternary loess deposition, Ili area, China. Quat. Int. 250, 84–92. https://doi.org/10.1016/j.quaint.2011.06.018.
Jia, J., Xia, D., Wang, B., Zhao, S., Li, G., Wei, H., 2013. The investigation of magnetic susceptibility variation mechanism of Tien Mountains modern loess: Pedogenic or wind intensity model? Quat. Int. 296, 141–148. https://doi.org/10.1016/j.quaint.2012.10.029.
Jia, J., Wang, B., Lu, C.C., Wang, Y.J., Zhu, L.D., Xia, D.S., 2019. New insights into the magnetic characteristics of high mountain loess in Central Asia and its paleoclimatic implications. Quat. Int. 502, 71–77. https://doi.org/10.1016/j.quaint.2019.01.031.
Jiang, Q.D., Yang, X.P., 2019. Sedimentological and geochemical composition of aeolian sediments in the Taklamakan Desert: implications for provenance and sediment supply mechanisms. J. Geophys. Res. Earth Surf. 124 (5), 1217–1237. https://doi.org/10.1029/2018jf004990.
Jilili, A., Ma, L., 2015. Overview of Central Asian Environment. China Meteorological Pres (in Chinese), Beijing, pp. 1–37.
Kang, S., Roberts, H.M., Wang, X., An, Z., Wang, M., 2015a. Mass accumulation rate changes in Chinese loess during MIS 2, and asynchrony with records from Greenland ice cores and North Pacific Ocean sediments during the Last Glacial Maximum. Aeolian Res. 19, 251–258. https://doi.org/10.1016/j.aeolia.2015.05.005.
Kang, S.G., Wang, X., Lu, Y., Liu, W.G., Song, Y., Wang, N., 2015b. A high-resolution quartz OSL chronology of the Talede loess over the past ∼30 ka and its implications for dust accumulation in the Ili Basin, Central Asia. Quat. Geochronol. 30, 181–187. https://doi.org/10.1016/j.quageo.2015.04.006.
Kang, S., Wang, X., Roberts, H.M., Duller, G.A.T., Song, Y., Liu, W., Zhang, R., Liu, X., Lan, J., 2020. Increasing effective moisture during the Holocene in the semiarid regions of the Yili Basin, Central Asia: Evidence from loess sections. Quat. Sci. Rev. 246, 106553. https://doi.org/10.1016/j.quascirev.2020.106553.
Karimi, A., Khademi, H., Kehl, M., Jalalian, A., 2009. Distribution, lithology and provenance of peridesert loess deposits in northeastern Iran. Geoderma 148 (3–4), 241–250. https://doi.org/10.1016/j.geoderma.2008.10.008.
Karimi, A., Frechen, M., Khademi, H., Kehl, M., Jalalian, A., 2011. Chronostratigraphy of loess deposits in northeast Iran. Quat. Int. 234 (1), 124–132. https://doi.org/10.1016/j.quaint.2009.08.002.
Kaskaoutis, D.G., Houssos, E.E., Rashki, A., Francois, P., Legrand, M., Goto, D., Bartzokas, A., Kambezidis, H.D., Takemura, T., 2016. The Caspian Sea-Hindu Kush Index (CasHKI): A regulatory factor for dust activity over southwest Asia. Glob. Planet. Chang. 137, 10–23. https://doi.org/10.1016/j.gloplacha.2015.12.011.
Kehl, M., 2010. Quaternary Loesses, Loess-Like Sediments, Soils and Climate Change in Iran. Schweizerbart Science Publishers, Gebr. Borntraeger Stuttgart, pp. 1–210.
Kehl, M., Sahvati, R., Ahmadi, H., Frechen, M., Skowronek, A., 2005. Loess paleosol-sequences along a climatic gradient in Northern Iran. Eiszeit. Gegenw. 55, 149–173.
Lai, Z.P., 2010. Chronology and the upper dating limit for loess samples from Luochuan section in the Chinese Loess Plateau using quartz OSL SAR protocol. J. Asian Earth Sci. 37 (2), 176–185. https://doi.org/10.1016/j.jseaes.2009.08.003.
Lauer, T., Frechen, M., Vlaminck, S., Kehl, M., Lehndorff, E., Shahriari, A., Khormali, F., 2017a. Luminescence-chronology of the loess palaeosol sequence Toshan, Northern Iran – A highly resolved climate archive for the last glacial–interglacial cycle. Quat. Int. 429, 3–12. https://doi.org/10.1016/j.quaint.2015.03.045.
Lauer, T., Vlaminck, S., Frechen, M., Rolf, C., Kehl, M., Sharifi, J., Lehndorff, E., Khormali, F., 2017b. The Agh Band loess-palaeosol sequence – A terrestrial archive for climatic shifts during the last and penultimate glacial–interglacial cycles in a semiarid region in northern Iran. Quat. Int. 429, 13–30. https://doi.org/10.1016/j.quaint.2016.01.062.
Lazarenko, A., Bolikhovskaya, N., Semenov, V., 1981. An attempt at a detailed stratigraphic subdivision of the loess association of the Tashkent region. Int. Geol. Rev. 23 (11), 1335–1346.
Lei, Y.B., Tian, L.D., Bird, B.W., Hou, J.Z., Ding, L., Oimahmadov, I., Gadoev, M., 2014. A 2540-year record of moisture variations derived from lacustrine sediment (Sasikul Lake) on the Pamir Plateau. Holocene 24 (7), 761–770. https://doi.org/10.1177/0959683614530443.
Li, B., Li, S.-H., 2011. Luminescence dating of K-feldspar from sediments: A protocol without anomalous fading correction. Quat. Geochronol. 6 (5), 468–479. https://doi.org/10.1016/j.quageo.2011.05.001.
Li, B., Li, S.-H., 2012. Luminescence dating of Chinese loess beyond 130 ka using the non-fading signal from K-feldspar. Quat. Geochronol. 10, 24–31. https://doi.org/10.1016/j.quageo.2011.12.005.
Li, Y., Song, Y., 2020. Discussion of the paper "Loess genesis and worldwide distribution" by Yanrong Li, Wenhui Shi, Adnan Aydin, et al. Earth-Sci. Rev. 103151 https://doi.org/10.1016/j.earscirev.2020.103151.
Li, C.X., Song, Y.G., Wang, Y.M., 2012. Distribution, age and dust sources of loess in the Ili basin. Earth Environ. 40 (3), 314–320 (in Chinese with Englishe abstract).
Li, G., Wen, L.J., Xia, D.S., Duan, Y.W., Rao, Z.G., Madsen, D.B., Wei, H.T., Li, F.L., Jia, J., Chen, F.H., 2015a. Quartz OSL and K-feldspar pIRIR dating of a loess/paleosol sequence from arid central Asia, Tianshan Mountains, NW China. Quat. Geochronol. 28, 40–53. https://doi.org/10.1016/j.quageo.2015.03.011.
Li, Y., Song, Y.G., Yan, L.B., Chen, T., An, Z.S., 2015b. Timing and spatial distribution of loess in Xinjiang, NW China. PLoS One 10 (5), e0125492. https://doi.org/10.1371/journal.pone.0125492.
Li, G.Q., Rao, Z.G., Duan, Y.W., Xia, D.S., Wang, L.B., Madsen, D.B., Jia, J., Wei, H.T., Qiang, M.R., Chen, J.H., Chen, F.H., 2016a. Paleoenvironmental changes recorded in a luminescence dated loess/paleosol sequence from the Tianshan Mountains, arid central Asia, since the Penultimate Glaciation. Earth Planet. Sci. Lett. 448, 1–12. https://doi.org/10.1016/j.epsl.2016.05.008.
Li, Y., Song, Y., Lai, Z., Li, H., An, Z., 2016b. Rapid and cyclic dust accumulation during MIS 2 in Central Asia inferred from loess OSL dating and grain-size analysis. Sci. Rep. 6, 32365. https://doi.org/10.1038/srep32365.
Li, G.Q., Chen, F.H., Xia, D.S., Yang, H., Zhang, X.J., Madsen, D., Oldknow, C., Wei, H.T., Rao, Z.G., Qiang, M.R., 2018a. A Tianshan Mountains loess-paleosol sequence indicates anti-phase climatic variations in arid central Asia and in East Asia. Earth Planet. Sci. Lett. 494, 153–163. https://doi.org/10.1016/j.epsl.2018.04.052.
Li, Y., Song, Y., Fitzsimmons, K., Chen, X., Zhang, Z., 2018b. New evidence for the provenance and formation of loess deposits in the Ili River Basin, Arid Central Asia. Aeolian Res. 35, 1–8. https://doi.org/10.1016/j.aeolia.2018.08.002.
Li, Y., Song, Y., Fitzsimmons, K.E., Chang, H., Orozbaev, R., Li, X., 2018c. Eolian dust dispersal patterns since the last glacial period in eastern Central Asia: insights from a loess-paleosol sequence in the Ili Basin. Clim. Past 14 (3), 271–286. https://doi.org/10.5194/cp-14-271-2018.
Li, Y., Song, Y., Qiang, M., Miao, Y., Zeng, M., 2019a. Atmospheric dust variations in the Ili Basin, Northwest China, during the last glacial period as revealed by a high Mountain Loess-paleosol sequence. J. Geophys. Res. Atmos. 124 (15), 8449–8466. https://doi.org/10.1029/2019jd030470.
Li, Y., Song, Y.G., Kaskaoutis, D.G., Chen, X.L., Mamadjanov, Y., Tan, L.C., 2019b. Atmospheric dust dynamics in southern Central Asia: Implications for buildup of Tajikistan loess sediments. Atmos. Res. 229, 74–85. https://doi.org/10.1016/j.atmosres.2019.06.013.
Li, Y., Song, Y.G., Yin, Q.Z., Han, L., Wang, Y.X., 2019c. Orbital and millennial northern mid-latitude westerlies over the last glacial period. Clim. Dyn. 53 (5–6), 3315–3324. https://doi.org/10.1007/s00382-019-04704-5.
Li, G., Xia, D., Appel, E., Lu, H., Wang, Y., Jia, J., Yang, X., 2020a. Characteristics of a relative paleointensity record from loess deposits in arid central Asia and chronological implications. Quat. Geochronol. 55, 101034. https://doi.org/10.1016/j.quageo.2019.101034.
Li, G.Q., Yang, H., Stevens, T., Zhang, X.J., Zhang, H.X., Wei, H.T., Zheng, W.P., Li, L.J., Liu, X.J., Chen, J.H., Xia, D.S., Oldknow, C., Ye, W., Chen, F.H., 2020b. Differential ice volume and orbital modulation of Quaternary moisture patterns between Central and East Asia. Earth Planet. Sci. Lett. 530, 115901. https://doi.org/10.1016/j.epsl.2019.115901.
Li, X.J., Zan, J.B., Yang, R.S., Fang, X.M., Yang, S.L., 2020c. Grain-size-dependent geochemical characteristics of Middle and Upper Pleistocene loess sequences from the Junggar Basin: Implications for the provenance of Chinese eolian deposits. Palaeogeogr. Palaeoclimatol. Palaeoecol. 538, 109458. https://doi.org/10.1016/j.palaeo.2019.109458.
Li, Y., Gholami, H., Song, Y., Fathabadi, A., Malakooti, H., Collins, A.L., 2020d. Source fingerprinting loess deposits in Central Asia using elemental geochemistry with Bayesian and GLUE models. Catena 194, 104808. https://doi.org/10.1016/j.catena.2020.104808.
Li, Y., Song, Y., Fitzsimmons, K.E., Chen, X., Prud'homme, C., Zong, X., 2020e. Origin of loess deposits in the North Tian Shan piedmont, Central Asia. Palaeogeogr. Palaeoclimatol. Palaeoecol. 559, 109972. https://doi.org/10.1016/j.palaeo.2020.109972.

Li, Y.R., Shi, W.H., Aydin, A., Beroya-Eitner, M.A., Gao, G.H., 2020f. Loess genesis and worldwide distribution. Earth-Sci. Rev. 201, 102947. https://doi.org/10.1016/j.earscirev.2019.102947.

Ling, Z.Y., Yang, S.L., Wang, X., Wang, J.P., Xia, D.S., Chen, F.H., 2020. Spatial-temporal differentiation of eolian sediments in the Yarlung Tsangpo catchment, Tibetan Plateau, and response to global climate change since the Last Glaciation. Geomorphology 357, 107104. https://doi.org/10.1016/j.geomorph.2020.107104.

Liu, Y., Shi, Z., Deng, C., Su, H., Zhang, W., 2012. Mineral magnetic investigation of the Talede loess–palaeosol sequence since the last interglacial in the Yili Basin in the Asian interior. Geophys. J. Int. 190 (1), 267–277. https://doi.org/10.1111/j.1365-246X.2012.05527.x.

Long, H., Shen, J., Chen, J., Tsukamoto, S., Yang, L., Cheng, H., Frechen, M., 2017. Holocene moisture variations over the arid central Asia revealed by a comprehensive sand-dune record from the central Tian Shan, NW China. Quat. Sci. Rev. 174, 13–32. https://doi.org/10.1016/j.quascirev.2017.08.024.

Lu, H., An, Z., 1998. Paleoclimatic significance of grain-size of loess-paleosol deposit in Chines Loess Plateau. Sci. China(Series D) 28 (3), 278–283.

Lu, H., Wang, X., Li, L., 2010. Aeolian sediment evidence that global cooling has driven late Cenozoic stepwise aridification in central Asia. Geol. Soc. Lond., Spec. Publ. 342 (1), 29–44. https://doi.org/10.1144/SP342.4.

Lu, H.H., Xu, Y.D., Niu, Y., Wang, Z., Wang, H., Zhao, J.X., Zhang, W.G., Zheng, X.M., 2016. Late Quaternary loess deposition in the southern Chaiwopu Basin of the northern Chinese Tian Shan foreland and its palaeoclimatic implications. Boreas 45 (2), 304–321. https://doi.org/10.1111/bor.12152.

Lu, H., Jia, J., Yin, Q., Xia, D., Gao, F., Liu, H., Fan, Y., Li, Z., Wang, X., Berger, A., Oimuhammadzoda, I., Gadoev, M., 2020. Atmospheric dynamics patterns in Southern Central Asia Since 800 ka revealed by loess-paleosol sequences in Tajikistan. Geophys. Res. Lett. 47 (17), e2020GL088320 https://doi.org/10.1029/2020gl088320.

Machalett, B., Frechen, M., Hambach, U., Oches, E.A., Zöller, L., Marković, S.B., 2006. The loess sequence from Remisowka (northern boundary of the Tien Shan Mountains, Kazakhstan)—Part I: Luminescence dating. Quat. Int. 152-153, 192–201. https://doi.org/10.1016/j.quaint.2005.12.014.

Machalett, B., Oches, E.A., Frechen, M., Zöller, L., Hambach, U., Mavlyanova, N.G., Marković, S.B., Endlicher, W., 2008. Aeolian dust dynamics in central Asia during the Pleistocene: Driven by the long-term migration, seasonality, and permanency of the Asiatic polar front. Geochem. Geophys. Geosyst. 9 (8). Q08Q09.doi:10.1029/2007gc001938.

Maher, B.A., 1998. Magnetic properties of modern soils and Quaternary loessic paleosols: paleoclimatic implications. Palaeogeogr. Palaeoclimatol. Palaeoecol. 137 (1), 25–54. https://doi.org/10.1016/S0031-0182(97)00103-X.

Maher, B.A., 2016. Palaeoclimatic records of the loess/palaeosol sequences of the Chinese Loess Plateau. Quat. Sci. Rev. 154, 23–84. https://doi.org/10.1016/j.quascirev.2016.08.004.

Mavlyanov, G.A., Kasymov, S.M., Shermatov, M.S., 1987. The Uzbekistan Loess, genesis and distribution. GeoJournal 15 (2), 145–150. https://doi.org/10.1007/BF00157940.

Miao, Y.F., Song, Y.G., Li, Y., Yang, S.L., Li, Y., Zhao, Y.T., Zeng, M.X., 2020. Late Pleistocene fire in the Ili Basin, Central Asia, and its potential links to paleoclimate change and human activities. Palaeogeogr. Palaeoclimatol. Palaeoecol. 547, 109700. https://doi.org/10.1016/j.palaeo.2020.109700.

Muhs, D.R., 2013a. The geologic records of dust in the Quaternary. Aeolian Res. 9, 3–48. https://doi.org/10.1016/j.aeolia.2012.08.001.

Muhs, D.R., 2013b. Loess and its Geomorphic, Stratigraphic, and Paleoclimatic Significance in the Quaternary. In: Shroder, J.F. (Ed.), Treatise on Geomorphology. Academic Press, San Diego, pp. 149–183.

Nobakht, M., Shahgedanova, M., White, K., 2019. New inventory of dust sources in Central Asia derived from the daily MODIS imagery, E3S Web of Conferences.

Obruchev, V.A., 1945. Loess Types and Their Origin. Am. J. Sci. 243 (5), 256–262. https://doi.org/10.2475/ajs.243.5.256.

Orlovsky, L., Orlovsky, N., Durdyev, A., 2005. Dust storms in Turkmenistan. J. Arid Environ. 60 (1), 83–97. https://doi.org/10.1016/j.jaridenv.2004.02.008.

Parviz, N., Shen, Z., Yunus, M., Zulqarnain, S., 2020. Loess deposits in southern Tajikistan (Central Asia): Magnetic properties and paleoclimate. Quat. Geochronol. 60, 101114. https://doi.org/10.1016/j.quageo.2020.101114.

Porter, S.C., An, Z.S., 1995. Correlation between climate events in the North-Atlantic and China during Last Glaciation. Nature 375 (6529), 305–308. https://doi.org/10.1038/375305a0.

Qin, J., Zhou, L., 2018. Luminescence dating of the Zeketai loess section in the Ili Basin, northwestern China: Methodological considerations. J. Asian Earth Sci. 155, 146–153. https://doi.org/10.1016/j.jseaes.2017.11.018.

Roe, G., 2009. On the interpretation of Chinese loess as a paleoclimate indicator. Quat. Res. 71 (2), 150–161. https://doi.org/10.1016/j.yqres.2008.09.004.

Rugenstein, J.K.C., Chamberlain, C.P., 2018. The evolution of hydroclimate in Asia over the Cenozoic: A stable-isotope perspective. Earth-Sci. Rev. 185, 1129–1156. https://doi.org/10.1016/j.earscirev.2018.09.003.

Rui, X., Li, B., Guo, Y., 2020. Testing the upper limit of luminescence dating based on standardised growth curves for MET-pIRIR signals of K-feldspar grains from northern China. Quat. Geochronol. 57, 101063. https://doi.org/10.1016/j.quageo.2020.101063.

Schaetzl, R.J., Bettis, E.A., Crouvic, O., Fitzsimmons, K.E., Grimley, D.A., Hambach, U., Lehmkuhl, F., Markovic, S.B., Mason, J.A., Owczarek, P., Roberts, H.M., Rousseau, D.D., Stevens, T., Vandenberghe, J., Zarate, M., Veres, D., Yang, S.L., Zech, M., Conroy, J.L., Dave, A.K., Faust, D., Hao, Q.Z., Obreht, I., Prud'homme, C., Smalley, I., Tripaldi, A., Zeeden, C., Zech, R., 2018. Approaches and challenges to the study of loess: Introduction to the Loess-Fest Special Issue. Quat. Res. 89 (3), 563–618. https://doi.org/10.1017/qua.2018.15.

Sha, Y.Y., Shi, Z.G., Liu, X.D., An, Z.S., Li, X.Z., Chang, H., 2018. Role of the Tian Shan Mountains and Pamir Plateau in Increasing Spatiotemporal Differentiation of Precipitation over Interior Asia. J. Clim. 31 (19), 8141–8162. https://doi.org/10.1175/Jcli-D-17-0594.1.

Shackleton, N.J., An, Z.S., Dodonov, A.E., Gavin, J., Kukla, G.J., Ranov, V.A., Zhou, L., 1995. Accumulation rate of loess in Tadjikistan and China: Relationship with global ice volume cycles. Quat. Proc. 4, 1–6.

Shi, Z.T., 2005. The Age Of Loess Sediments in Yili srea of Xinjiang and its Paleoenvironment Significances. Institute of Earth Environment, Chinese Academy of Sciences, Xi'an.

Shu, P.X., Li, B.S., Wang, H., Cheng, P., An, Z.S., Zhou, W.J., Zhang, D.D., Dodson, J., Niu, D.F., Si, Y.J., Wen, X.H., Qiu, Y.H., 2018. Abrupt environmental changes during the last 30 kyr in the southern margin of the Taklimakan Desert, a record from an oasis. Quat. Sci. Rev. 201, 29–43. https://doi.org/10.1016/j.quascirev.2018.09.036.

Singhvi, A.K., Bluszcz, A., Bateman, M.D., Rao, M.S., 2001. Luminescence dating of loess–palaeosol sequences and coversands: methodological aspects and palaeoclimatic implications. Earth-Sci. Rev. 54 (1), 193–211. https://doi.org/10.1016/S0012-8252(01)00048-4.

Smalley, I.J., Mavlyanova, N.G., Rakhmatullaev, K.L., Shermatov, M.S., Machalett, B., O'Hara Dhand, K., Jefferson, I.F., 2006. The formation of loess deposits in the Tashkent region and parts of Central Asia; and problems with irrigation, hydrocollapse and soil erosion. Quat. Int. 152-153, 59–69. https://doi.org/10.1016/j.quaint.2005.12.002.

Song, Y., Shi, Z., Fang, X., Nie, J., Naoto, I., Qiang, X., Wang, X., 2010. Loess magnetic properties in the Ili Basin and their correlation with the Chinese Loess Plateau. Sci. China Earth Sci. 53 (3), 419–431. https://doi.org/10.1007/s11430-010-0011-5.

Song, Y.G., Li, C.X., Zhao, J.D., Cheng, P., Zeng, M.X., 2012. A combined luminescence and radiocarbon dating study of the Ili loess, Central Asia. Quat. Geochronol. 10, 2–7. https://doi.org/10.1016/j.quageo.2012.04.005.

Song, Y.G., Chen, X.L., Qian, L.B., Li, C.X., Li, Y., Li, X.X., Chang, H., An, Z.S., 2014a. Distribution and composition of loess sediments in the Ili Basin, Central Asia. Quat. Int. 334-335, 61–73. https://doi.org/10.1016/j.quaint.2013.12.053.

Song, Y.G., Fang, X.M., King, J.W., Li, J.J., Naoto, I., An, Z.S., 2014b. Magnetic parameter variations in the Chaona loess/paleosol sequences in the central Chinese Loess Plateau, and their significance for the middle Pleistocene climate transition. Quat. Res. 81 (3), 433–444. https://doi.org/10.1016/j.yqres.2013.10.002.

Song, Y.G., Lai, Z.P., Li, Y., Chen, T., Wang, Y.X., 2015. Comparison between luminescence and radiocarbon dating of late Quaternary loess from the Ili Basin in Central Asia. Quat. Geochronol. 30, 405–410. https://doi.org/10.1016/j.quageo.2015.01.012.

Song, Y.G., Luo, D., Du, J.H., Kang, S.G., Cheng, P., Fu, C.F., Guo, X.H., 2018a. Radiometric dating of late Quaternary loess in the northern piedmont of South Tianshan Mountains: Implications for reliable dating. Geol. J. 53, 417–426. https://doi.org/10.1002/gj.3129.

Song, Y.G., Zeng, M.X., Chen, X.L., Li, Y., Chang, H., An, Z.S., Guo, X.H., 2018b. Abrupt climatic events recorded by the Ili loess during the last glaciation in Central Asia: Evidence from grain-size and minerals. J. Asian Earth Sci. 155, 58–67. https://doi.org/10.1016/j.jseaes.2017.10.040.

Song, Y., Zong, X., Li, Y., Rustam, O., Mamadjanov, Y., Aminov, J., 2019. Loess sediments and rapid climate oscillation during the last glacial period in the westerlies-dominated Central Asia. Quat. Sci. 39 (3), 535–548. https://doi.org/10.11928/j.issn.1001-7410.2019.03.02 (In Chinese with English abstract).

Sorrel, P., Oberhänsli, H., Boroffka, N., Nourgaliev, D., Dulski, P., Röhl, U., 2007. Control of wind strength and frequency in the Aral Sea basin during the late Holocene. Quat. Res. 67 (3), 371–382. https://doi.org/10.1016/j.yqres.2006.12.003.

Steffensen, J.P., 1997. The size distribution of microparticles from selected segments of the Greenland Ice Core Project ice core representing different climatic periods. J. Geophys. Res. Oceans 102 (C12), 26755–26763. https://doi.org/10.1029/97jc01490.

Sun, J.M., 2002. Source regions and formation of the loess sediments on the high mountain regions of Northwestern China. Quat. Res. 58 (3), 341–351. https://doi.org/10.1006/qres.2002.2381.

Sun, H.Y., Song, Y.G., Chen, X.L., Cheng, L.Q., Liu, H.F., 2020. Holocene dust deposition in the Ili Basin and its implications for climate variations in Westerlies-dominated Central Asia. Palaeogeogr. Palaeoclimatol. Palaeoecol. 550, 109743. https://doi.org/10.1016/j.palaeo.2020.109731.

Thiel, C., Buylaert, J.-P., Murray, A., Terhorst, B., Hofer, I., Tsukamoto, S., Frechen, M., 2011. Luminescence dating of the Stratzing loess profile (Austria) – Testing the potential of an elevated temperature post-IR IRSL protocol. Quat. Int. 234 (1), 23–31. https://doi.org/10.1016/j.quaint.2010.05.018.

Thomsen, K.J., Murray, A.S., Jain, M., Bøtter-Jensen, L., 2008. Laboratory fading rates of various luminescence signals from feldspar-rich sediment extracts. Radiat. Meas. 43 (9), 1474–1486. https://doi.org/10.1016/j.radmeas.2008.06.002.

Tian, S., Sun, J., Zhang, Z., Abdulov, S., Cao, M., Gadoev, M., Oimahmadov, I., 2021. Loess deposits in the Tajik Basin, Central Asia: chronology, provenance and palaeoclimatic implications since the Last Glacial. Boreas 50 (1), 147–166. https://doi.org/10.1111/bor.12467.

Vandenberghe, J., Huijzer, B.S., Mücher, H., Laan, W., 1998. Short climatic oscillations in a western European loess sequence (Kesselt, Belgium). J. Quat. Sci. 13 (5), 471–485 doi:10.1002/(SICI)1099-1417(1998090)13:5<471::AID-JQS401>3.0.CO;2-T.

Vandenberghe, J., Renssen, H., Huissteden, K.V., Nugteren, G., Konert, M., Lu, H., Dodonov, A., Buylaert, J.P., 2006. Penetration of Atlantic westerly winds into

Central and East Asia. Quat. Sci. Rev. 25 (17–18), 2380–2389. https://doi.org/10.1016/j.quascirev.2006.02.017.

Vlaminck, S., Kehl, M., Lauer, T., Shahriari, A., Sharifi, J., Eckmeier, E., Lehndorff, E., Khormali, F., Frechen, M., 2016. Loess-soil sequence at Toshan (Northern Iran): Insights into late Pleistocene climate change. Quat. Int. 399, 122–135. https://doi.org/10.1016/j.quaint.2015.04.028.

Vlaminck, S., Kehl, M., Rolf, C., Franz, S.O., Lauer, T., Lehndorff, E., Frechen, M., Khormali, F., 2018. Late Pleistocene dust dynamics and pedogenesis in Southern Eurasia – Detailed insights from the loess profile Toshan (NE Iran). Quat. Sci. Rev. 180, 75–95. https://doi.org/10.1016/j.quascirev.2017.11.010.

Wang, E., Wan, J.L., Liu, J.Q., 2003. Late Cenozoic geological evolution of the foreland basin bordering the West Kunlun range in Pulu area: Constraints on timing of uplift of northern margin of the Tibetan Plateau. J. Geophys. Res. Solid Earth 108 (B8), 2401. https://doi.org/10.1029/2002jb001877.

Wang, X., Wei, H.T., Taheri, M., Khormali, F., Danukalova, G., Chen, F.H., 2016. Early Pleistocene climate in western arid central Asia inferred from loess-palaeosol sequences. Sci. Rep. 6, 20560. https://doi.org/10.1038/srep20560.

Wang, L.B., Jia, J., Li, G.Q., Li, Z.J., Wang, X., Chen, F.H., 2018. Fine-grained quartz OSL dating chronology of loess sequence from southern Tajikistan: Implications for climate change in arid central Asia during MIS 2. J. Asian Earth Sci. 155, 116–123. https://doi.org/10.1016/j.jseaes.2017.11.001.

Wang, L.B., Jia, J., Xia, D.S., Liu, H., Gao, F.Y., Duan, Y.W., Wang, Q., Xie, H.C., Chen, F. H., 2019a. Climate change in arid central Asia since MIS 2 revealed from a loess sequence in Yili Basin, Xinjiang, China. Quat. Int. 502, 258–266. https://doi.org/10.1016/j.quaint.2018.02.032.

Wang, L.B., Jia, J., Zhao, H., Liu, H., Duan, Y.W., Xie, H.C., Zhang, D.D., Chen, F.H., 2019b. Optical dating of Holocene paleosol development and climate changes in the Yili Basin, arid central Asia. Holocene 29 (6), 1068–1077. https://doi.org/10.1177/0959683619831432.

Wolff, C., Plessen, B., Dudashvilli, A.S., Breitenbach, S.F.M., Cheng, H., Edwards, L.R., Strecker, M.R., 2016. Precipitation evolution of Central Asia during the last 5000 years. The Holocene 27 (1), 142–154. https://doi.org/10.1177/0959683616652711.

Wu, F.L., Fang, X.M., Miao, Y.F., 2020. Aridification history of the West Kunlun Mountains since the mid-Pleistocene based on sporopollen and microcharcoal records. Palaeogeogr. Palaeoclimatol. Palaeoecol. 547, 109680. https://doi.org/10.1016/j.palaeo.2020.109680.

Xiao, J., Porter, S.C., An, Z., Kumai, H., Yoshikawa, S., 1995. Grain size of quartz as an indicator of winter monsoon strength on the Loess Plateau of central China during the last 130,000 yr. Quat. Res. 43 (1), 22–29. https://doi.org/10.1016/j.quaint.2020.05.039.

Yang, S.L., Ding, F., Ding, Z.L., 2006. Pleistocene chemical weathering history of Asian arid and semi-arid regions recorded in loess deposits of China and Tajikistan. Geochim. Cosmochim. Acta 70 (7), 1695–1709. https://doi.org/10.1016/j.gca.2005.12.012.

Yang, S.L., Forman, S.L., Song, Y.G., Pierson, J., Mazzocco, J., Li, X.X., Shi, Z.T., Fang, X. M., 2014. Evaluating OSL-SAR protocols for dating quartz grains from the loess in Ili Basin, Central Asia. Quat. Geochronol. 20, 78–88. https://doi.org/10.1016/j.quageo.2013.11.004.

Yang, H., Li, G., Huang, X., Wang, X., Zhang, Y., Jonell, T.N., Jin, M., Chen, C., Zhao, W., Zhang, H., Wang, Z., Deng, Y., 2020a. Loess depositional dynamics and paleoclimatic changes in the Yili Basin, Central Asia, over the past 250 ka. Catena 195, 104881. https://doi.org/10.1016/j.catena.2020.104881.

Yang, S.L., Li, D.X., Liu, N.N., Zan, J.B., Liu, W.M., Kang, J., Murodov, A., Fang, X.M., 2020b. Quartz optically stimulated luminescence dating of loess in Tajikistan and its paleoclimatic implications for arid Central Asia since the Lateglacial. Palaeogeogr. Palaeoclimatol. Palaeoecol. 556, 109881. https://doi.org/10.1016/j.palaeo.2020.109881.

Ye, W., 2000. The mineral characteristics of loess and depositional environment in Yili area, Xinjinag. Arid Zone Res. 17 (4), 1–10 (in Chinese).

Youn, J.H., Seong, Y.B., Choi, J.H., Abdrakhmatov, K., Ormukov, C., 2014. Loess deposits in the northern Kyrgyz Tien Shan: Implications for the paleoclimate reconstruction during the Late Quaternary. Catena 117, 81–93. https://doi.org/10.1016/j.catena.2013.09.007.

Yu, L., Lai, Z., 2012. OSL chronology and palaeoclimatic implications of aeolian sediments in the eastern Qaidam Basin of the northeastern Qinghai-Tibetan Plateau. Palaeogeogr. Palaeoclimatol. Palaeoecol. 337-338, 120–129. https://doi.org/10.1016/j.palaeo.2012.04.004.

Zan, J.B., Fang, X.M., Yang, S.L., Nie, J.S., Li, X.Y., 2010. A rock magnetic study of loess from the West Kunlun Mountains. J. Geophys. Res. 115, B10101. https://doi.org/10.1029/2009jb007184.

Zan, J., Fang, X., Nie, J., Yang, S., Song, C., Dai, S., 2011. Magnetic properties of surface soils across the southern Tarim Basin and their relationship with climate and source materials. Chin. Sci. Bull. 56 (3), 290–296. https://doi.org/10.1007/s11434-010-4210-4.

Zan, J., Fang, X., Yang, S., Yan, M., 2013. Evolution of the arid climate in High Asia since ~1 Ma: Evidence from loess deposits on the surface and rims of the Tibetan Plateau. Quat. Int. 313-314, 210–217. https://doi.org/10.1016/j.quaint.2013.03.012.

Zan, J., Fang, X., Kang, J., Li, X., Yan, M., 2020. Spatial and altitudinal variations in the magnetic properties of eolian deposits in the northern Tibetan Plateau and its adjacent regions: Implications for delineating the climatic boundary. Earth-Sci. Rev. 208, 103271. https://doi.org/10.1016/j.earscirev.2020.103271.

Zeng, M., Song, Y., Li, Y., Fu, C., Qiang, X., Chang, H., Zhu, L., Zhang, Z., Cheng, L., Yang, G., 2019. The relationship between environmental factors and magnetic susceptibility in the Ili loess, Tianshan Mountains, Central Asia. Geol. J. 54 (4), 1889–1901. https://doi.org/10.1002/gj.3182.

Zeng, M., Song, Y., Yang, H., Li, Y., Cheng, L., Li, F., Zhu, L., Wu, Z., Wang, N., 2021. Quantifying proportions of different material sources to loess based on a grid search and Monte Carlo model: A case study of the Ili Valley, Central Asia. Palaeogeogr. Palaeoclimatol. Palaeoecol. 565 https://doi.org/10.1016/j.palaeo.2020.110210.

Zhang, J.R., Zhou, X.Y., Long, H., 2020. Late Quaternary loess accumulation at the Rudak section in Uzbekistan, central Asia: Chronology and palaeoclimate implications. Palaeogeogr. Palaeoclimatol. Palaeoecol. 547, 109695. https://doi.org/10.1016/j.palaeo.2020.109695.

Zhao, H., Li, S., Li, B., Li, G., 2015. Holocene climate changes in westerly-dominated areas of central Asia: Evidence from optical dating of two loess sections in Tianshan Mountain, China. Quat. Geochronol. 30, 188–193. https://doi.org/10.1016/j.quageo.2015.04.002.

Zhou, L.P., Oldfield, F., Wintle, A.G., Robinson, S.G., Wang, J.T., 1990. Partly Pedogenic Origin of Magnetic Variations in Chinese Loess. Nature 346 (6286), 737–739. https://doi.org/10.1038/346737a0.

Zhou, L.P., Dodonov, A.E., Shackleton, N.J., 1995. Thermoluminescence dating of the Orkutsay loess section in Tashkent Region, Uzbekistan, Central Asia. Quat. Sci. Rev. 14 (7–8), 721–730. https://doi.org/10.1016/0277-3791(95)00056-9.

Zong, X.L., Dong, J.B., Cheng, P., Song, Y.G., Liu, W.G., Li, Y., Lan, J.H., 2020. Terrestrial mollusk records in the loess sequences from eastern Central Asia since the last deglaciation and their paleoenvironmental significance. Palaeogeogr. Palaeoclimatol. Palaeoecol. 556, 109890. https://doi.org/10.1016/j.palaeo.2020.109890.

Zykin, V.S., Zykina, V.S., 2015. The middle and late pleistocene loess-soil record in the Iskitim area of Novosibirsk Priobie, south-eastern West Siberia. Quat. Int. 365, 15–25. https://doi.org/10.1016/j.quaint.2014.07.011.